UNIVERSITA' DEGLI STUDI DI NAPOLI FEDERICO II

FACOLTA' DI INGEGNERIA

DOTTORATO IN INGEGNERIA ELETTRICA XX° ciclo

TESI DI DOTTORATO IN:

PROTON EXCHANGE MEMBRANE FUEL CELL ANALYSIS AND MODEL FOR ELECTRIC POWER APPLICATIONS

TUTOR:
Ch.mo Prof. Elio Chiodo

CANDIDATO:
Ing. Antonio Maria Ciro Zingariello

COORDINATORE DEL DOTTORATO
Ch.mo Prof. Guido Carpinelli

Anno Accademico 2006-2007

INDEX

INTRODUCTION

As shown by the growing number of paper focusing in research, development and applications, Fuel Cells (FC) currently are attracting the interest of more and more scientists. These sources are able to provide electric energy efficiently, respecting environmental constraints. These characteristics, and the possibility of refueling the cell with different fuels, are making for an interest in electric power applications sources. In the sector of electric power generation, regulation, power quality and environment issues are increasing the research into using Fuel Cells efficiently. In the field of Electric Vehicles design, the research of on-board electrical sources, characterized by high energy density, seems to favor the analysis and application of FC sources respect to electrochemical accumulator sources. Because of this, several manufacturers are currently intensively developing generation systems, basically constituted by a FC electrical source and a converter, able to adapt the Fuel Cell stack operating conditions to the requirements of the electrical system, Fig. 1 [1]-[2].

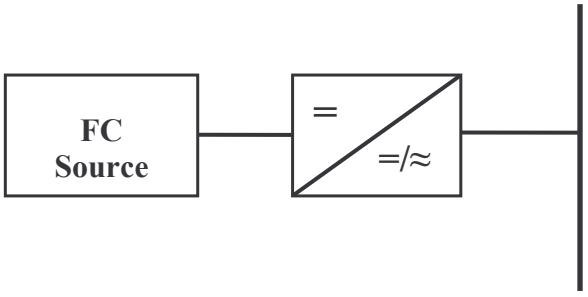

Fig. 1 - Electric power system FC source-based

This technology is not new, but just some of the fundamental difficulties have been overcome recently, so that these sources are becoming more feasible and are gradually commercialized.

For these reasons, polymeric electrolyte membrane (PEM) FC are largely treated by current literature, by growing importance on its electrical equivalent model, in order to improve a reliable management of system including fuel PEM FC.

CHAPTER I – FUEL CELL MISSION

Technological target for engineering applications

Current energy landscape shows weighty lacks not only in primary energetic sources, but also in capability of storage and handling of them. In fact both an optimal use of energetic sources, and an helpful storage system, could solve a fundamental part of actual energetic problems.

In this pattern, the Fuel Cell (FC) stacks have received heightened attention in the last few years. This is particularly due to their high electrical and overall efficiency (up to 80% for cogeneration of heat and power), low aggression to the environment, excellent dynamic response, and superior reliability and durability.

Among the various FC models actually available, the Proton Exchange Membrane Fuel Cell (PEMFC) seems a promising source to be used in residences, industries, and small- and large-scale distributed generation systems. The main characteristics of PEMFC stacks are: (*i*) they produce water as a residue; (*ii*) they have high efficiency when compared to thermal generation; (*iii*) they operate at low temperatures (up to 90 °C), which allows a fast start-up; and, (*iv*) they use a solid polymer as the electrolyte, which reduces concerns related to construction, transportation, and safety. From the electrical engineering viewpoint, the importance of a good Fuel Cell model is related to: the facility of tests of the fuel cell controllers; evaluation of the available power and energy for a certain load profile; and, evaluation of the needs for hydrogen and additional storage systems. Also, in power generation systems, the dynamic response is of extreme importance for the control planner and system management, especially when there is injection of energy into the network.

FC sources seems able to present significant challenges not only in great static energy storage application, but also in the transportation sector. In fact its great energy storage capacity make it a good alternative to traditional fuel, that is principal cause of earth pollution.

FC powered vehicles have likely to be hybrid electric vehicles because hybrid power sources composed of fuel cells and secondary batteries combine the high power energy density of clean fuel cells and the high energy quick available power density of batteries.

The hybridization could compensate limited transient response capability of FC systems and provide fuel economy improvement. The design of hybrid system depends on the modalities of energy consumption during working conditions and might include constraints on: mass, volume, life cycles, ability to operate well at sub-zero temperatures, charge and discharge rates.

Hybridization with Electrochemical Energy Storage (EES) technologies, including lead-acid, nickel-metal hydride, lithium-ion, could provide valid alternatives. To take advantage of the potential benefits, it is necessary to define the attributes of the EES system. Hybridizing FC vehicles with EES can produce several benefits, including capturing regenerative braking energy, enhancing fuel economy, providing flexible operating strategy, and lowering the cost per unit power. Moreover, FC source can be downsized and operate more efficiently.

In order to size vehicle's primary (FC) and secondary (EES) power sources, the roles of secondary power system should be established. EES, for instance, could be able for: 1)

traction power during FC start-up; 2) acceleration performance; 3) power-assist during drive cycles; 4) electrical auxiliary loads; 5) regenerative braking energy recapture. In particular, recovering the energy through regenerative breaking is an effective approach for improving vehicle driving range.

The hybrid configuration decreases the stress on the FC, accordingly smoothes source voltage peaks and decreases internal power losses. In order to fulfil load requirements in terms of maximum power and stored energy of driving conventional cycles, the integration of FC and battery in a Hybrid Electrical Vehicle (HEV) seems to be more convenient.

To define the modalities of interaction of the sources constituting the hybrid power system, it is necessary to investigate on their performances. Moreover, assigned the main requirements of the vehicle, special considerations must be taken into account when integrating such a hybrid system to achieve optimal performance.

Normally, the electric load profile consists of high peaks due to repetitive accelerations and decelerations. The resulting current surges act to age the power sources. FC source is characterized by ageing mechanisms on electrodes and membrane, which leads to lower power and ultimately premature failure.

Today, the durability of FC (in particular the Polymer Electrolyte Membrane (PEM) FC, used in vehicle applications) is one of the major barrier to the commercialization. In fact, commercial viability relates on reducing lifetime cost and improving power density, reliability and durability of the FC components.

FC durability is difficult to quantify and improve, not only because of the quantity and

duration (i.e., up to several thousand hours or more) of testing required, but also because the FC stack is a system of components, electrocatalysts, membranes, gas diffusion layers, and bipolar plates, for which the degradation mechanisms, component interactions and effects of operating conditions are not fully understood [2,3]. Thus, individual components must be well characterized during durability testing to determine and quantify degradation mechanisms that occur over long periods.

Due to the absence of moving parts, FC is an inherently reliable system, but can be prone to material degradation from the presence of: reactants, catalyst, electrical potential and current density, operating conditions, including temperature and pressure ranges. Several tests are now addressed to measure property changes in FC components during long-term testing (focusing on: Membrane-electrode structure, electrocatalyst activity and stability, Gas diffusion layer hydrophobicity, Corrosion products).

One of these test is very useful not only in search field, but above all in diagnostic and real time analysis: it is the Electrochemical Impedance Spectroscopy method (EIS), that will be largely treated in the third and fourth chapter. It is based on monitoring, at different frequency, the system impedance variation due to age or fault occurring of the cell. The fundamental property of this method, which has been often used for electrochemical accumulator system, is its non-invasive nature that doesn't modifies system equilibrium and thus gives reliable data. Moreover it is very simple and implementation costs are very cheap, so that it can be used for widespread real time diagnostic in order to show the actual system state and to predict fault occurrences.

All tests aim to identify the degradation modes, related to: the kinetic or activation loss in the anode or cathode catalyst, the loss of apparent catalytic activity, the ohmic or resistive increases in the membrane or other components, the loss of conductivity, the decrease in the mass transfer rate of in the reactants flow channel or electrode, the loss of mass transfer rate of reactants. Mainly, the loss of active catalyst surface area is caused by catalyst sintering and/or detaching of clusters from the catalyst layer surface. The decrease in active area occurs primarily in the cathode catalyst. The failure of Membrane Exchange Assembly (MEA) is due to the hydrogen cross-over; the small holes which appear in the membrane decrease the FC performance rapidly. Physical and functional attributes are reviewed for recently developed products that satisfy emerging requirements including stronger, more durable membranes, and polymer dispersions of higher quality and consistency for catalyst inks and film formation. FC stack lifetime is dependent on how the components and interacting conditions are designed and managed. Lifetime requirements vary significantly, ranging from 2000 to 5000 operating hours for car applications, up to 20000 operating hours for bus applications and up to 40000 operating hours for stationary applications.

Examining the performances of several elementary cells, it is possible to recognize various models of aging. In particular, the most of these assess the cell aging by means of a linear model [1,2,3]. The model introduces a degradation coefficient, ϕ, which normally depends on the instantaneous operating current. The lower the operating current densities are, the lower the degradation coefficient is. Examining the

experimental behaviour of several MEAs, it is possible to recognize that the degradation coefficient varies in the range 5-50 μV/hr.

Assuming the linear model, the degradation rate requirements are normally set based on the Beginning Of Life (BOL) and End Of Life (EOL) performance requirements; the lifetime durability requirements can be assessed in terms of operational hours. For instance, in fig.2, according to the analytical model of (1), there are reported, for several operative hours, the output power curves of a PEM FC (30 cells and ϕ=30 μV/hr) as function of current density (normalized on the source maximum current density). The curves of power are normalized to the peak power of the BOL. The results focus on the action of the degradation mechanisms, which, comparing the maximum available power of the BOL to the maximum available power of 4500 h, can determine an impressive drop, higher that 30%.

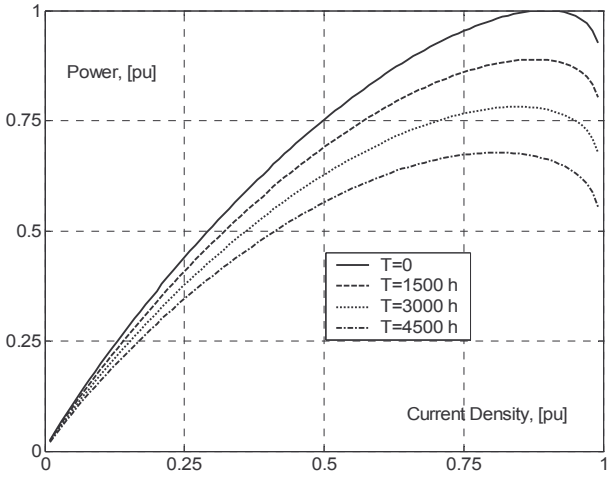

Fig 1.1 – Derating of FC output power as a function of current density, due to degradation mechanisms

Hybrid-electric vehicles require a compact, high energy-density electrical source to provide both high power and high energy. The necessity of adopting storage sources is imposed by the extreme performances that automotive vehicle requires and by the limits that these technology shows. In hybrid sources, EES can help the FC source supplying the high power demand and absorbing the energy providing by the load.

In order to provide an useful auxiliary device to FC source, electrochemical battery accumulators, behaving as energy buffer, can offset peaks of power and than allow to undersize FC. They can be also indispensable in order to store excess of power during prolonged and repetitive braking. There is potential to improve the performance, reliability, and extend the operating environment of all hybrid-electric power trains. Typical advantages are longer range for quiet operation, better acceleration, higher fuel mileage, and lower maintenance.

The simplest hybrid configuration is formed by connecting the fuel cell and the battery directly. In contrast to simple power sources (a battery alone or a fuel cell alone), such a passive hybrid demonstrates a longer run time and a higher power capability [3, 4]. The hybrid configuration also decreases the stress on the fuel cell and accordingly smoothes the hybrid source terminal voltage and decreases internal power losses [5, 7]. However, such hybrid sources have several disadvantages. First, the battery stack terminal voltage must match the nominal voltage of the fuel cell, which limits the battery pack design. Secondly, since the power distribution between the fuel cell and the battery is passively determined by the impedance characteristics of each component, the hybrid source performance may be unnecessarily limited by one of those two components. For

example, the peak power capability of the hybrid may be restricted by the fuel cell when it first reaches its safe power limit even while the output power of the battery is still well below its maximum.

The required maximum power and driving cycle energy must be furnished by FC and battery sources in several amounts. If the sources are directly coupled ("passive" configuration), the capacity action of the hybrid source to the requirements is influenced by the parameters of each source and by their interaction modalities; the intrinsic characteristics of physical coupling make the hybrid source performances lower than to the sum of the performances of each source. Integrating the sources by means of dedicated converter ("active configuration"), it is possible to control the sources' action, optimizing the global action: assuming minimal the loss of efficiency due to the converters, the hybrid source performances are equal to the sum of the sources performances [6,7].

One important advantage of the active hybrid power sources is that they can increase the peak output power greatly over the fuel cell alone or the passive hybrid. A well controlled active hybrid fuel cell/battery power source can maximize the usage of the power capability of each component. In other words, the fuel cell and the battery can be controlled to generate the maximum power of each concurrently. In contrast, in the passive hybrid, as the load power demand increases, either the fuel cell rises to its maximum power capability before the battery or vice versa; consequently the hybrid source power capability is limited. This is because in the passive hybrid, the fuel cell is

connected to the battery directly and thus the power sharing between the fuel cell and the battery is passively determined by component characteristics.

The objective of the control strategy can be related to operate the vehicle with the highest fuel economy, while maintaining specified vehicle performance. In order to maintain the sources in their own limits and to reduce EES size and hydrogen consumption, an energy management must be considered. To provide a power demand with the FC and EES an algorithm must manage the interaction, satisfying technical constraints and power reference. The technical constraints are defined by both the source behaviours and imposed control strategy. The power references are related to the autonomy (in km or in continued operating time), which determines the needs of on-board energy and maximum required power.

The concept of power management normally assumes that the FC source provides the driving cycle energy, while the EES provides the peak or transient power. This is achieved by controlling the FC source to operate within prefixed efficiency range and effectively capturing the regenerative energy by controlling the state of charge of the battery [8].

The design of the hybrid source is the synthesis of a complex minimization process, which must take into account the performances and operational constraints of the constituting sources. The capability of the hybrid source could be expressed in terms of maximum power (P_H) and usable energy (E_H), which must be at least equal to the values of the assumed driving cycle. Independently of the power source type, the vehicle power requirements is normally estimated using a dynamic model of vehicle physical

dimensions and weight. The energy and power required to satisfy the performances are frequently estimated using dedicated software (i.e. ADVISOR) and, normally, include the losses of the mechanical and electrical systems (transmission, motor, power electronics, etc.). Thus, the energetic requirements are a function of the driving schedule and, in literature, several are the reported reference driving cycles [8].

The target pursued by the designer of an hybrid power source for on-board application is choosing the component sizes which fulfil power and energy constraints and minimize the mass. In order to assure a minimum level of reliability it is necessary taking into account component degradation mechanisms.

Aiming to describe the incidence of the FC degradation on the hybrid source design model, a minimization procedure, able to design the hybrid source controlling the FC to operate within reduced range of efficiency, is proposed. The study of this issue is still in an early phase: data are scarce and uncertainty. However, it could be already interesting to develop former considerations on rules of thumbs, helpful to build sensibility on the problem. According to this context, a mathematical expression of design algorithm can be summarized as follow:

$$\left\{\begin{array}{c} \min(M_{FC} + A * M_{Hydr} + M_{Batt}) \\ P_V \le P_H = p_{FC}(t) M_{FC} + p_{Batt} M_{Batt} \\ E_V \le E_H = e_{Hydr} \eta M_{Hydr} \\ P_{mean} \le p_{FC}(t) M_{FC} \end{array}\right\} \quad (1)$$

where M_j is the mass of the j sources, M_{Hydr} is the mass of the hydrogen; e_j is the energy densities of j source; P_V, P_{mean} and E_V are, respectively, the maximum and mean powers and energy required by the vehicle to realize the driving cycle; A is a coefficient which related the hydrogen storing system to the stored hydrogen; η takes in to account the ratio among the usable and the storage hydrogen; p_j is the power densities of j source. According to the considerations reported in section 2, the power density of the FC source depends on the operating time.

The procedure has the input data of the 10-15 driving schedule reported in [8], and minimizes, at several operating time, the on-board hybrid source mass according to the data of tab.1 and 2. The results focus on a FC stack made up of 30 elementary cells. During the considered operating time of 4500 h, the analyses are performed assuming that the FC source derates with linear coefficients of 30 and 50 μV/hr. According to these assumption, the degradation mechanisms act on the FC power density as reported in fig.1.2

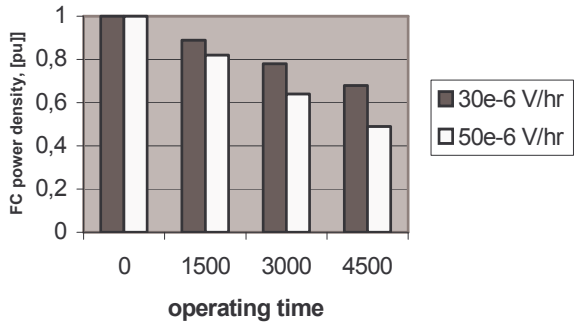

Fig.1.2 – FC power density as function of operating interval, for degradation coefficients of 30 and 50 μV/hr

The degradation coefficient acts on the design determining the oversize of the FC source. Observing fig.1.3, it is possible to note how, to assure the respect of the technical performances also for long operating time, the higher degradation coefficient of 50 μV/hr can also cause the design a FC source to be two times of the initial rate. The more is the reference time, i.e. the time that the FC operates without maintenance or replacement, the higher must be the on board FC rate.

$\mathbf{P_V}$	34 kW
$\mathbf{E_V}$	750 kWh
$\mathbf{P_{mean}}$	4.2 kW
$\mathbf{_{pFC}(t=0)}$	0.5 kW/kg
$\mathbf{e_{Hydr}}$	23 kWh/kg
A	20
η	0.93

Tab. 1.1 – Parameters of analytical model

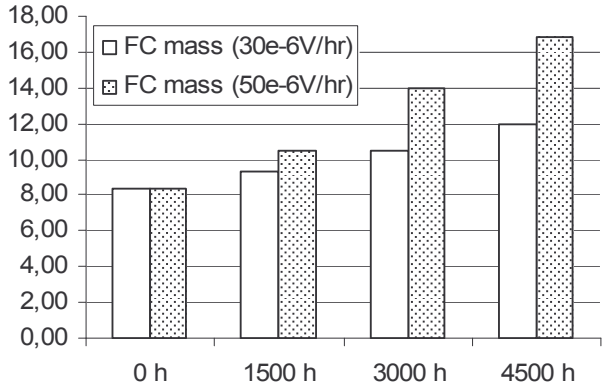

Fig.1.3 – Histogram of FC minimized masses, [kg], at various operating times

It is also interesting to observe the relative incidence of the weight of the FC source respect to the battery ones, fig.1.4. When there are used Pb battery, the lower battery power density makes the FC mass variation non significant (less than 5%), whereas, when there are suited higher power density battery (i.e. Li or Ni/MH), the incidence of the FC mass variation can be assessed of about 20 %, determining the significant increase of the on-board hybrid source weight. So that, for these kinds the suit of a FC source characterised by reduced degradation coefficient can result very significant in the hybrid source design.

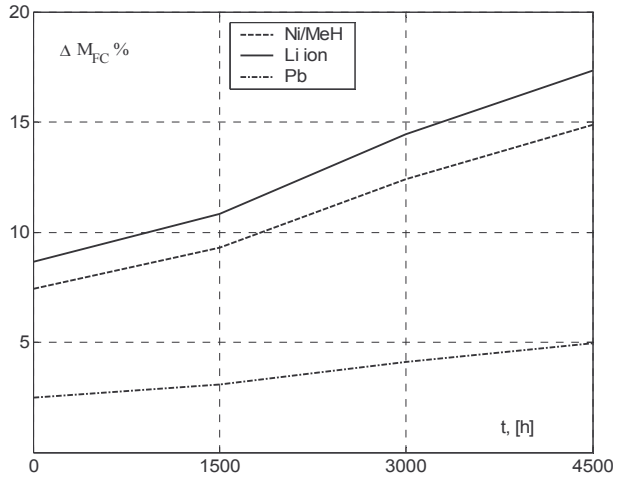

Fig.1.4 – FC mass per cent design as function of operating time

In order to improve the hybrid power system performance in terms of weight it would be useful increasing the source with the highest power density. In our case it is the FC, that is characterised by 1.5 kW/kg versus the 0.35 kW/kg of the best electrochemical battery, that is Lithion one. Unfortunately this condition would be unfavourable for energetic efficiency and good operating of the system, because it would mean reducing the buffer rule of battery and thus compelling the FC to work at variable and stressing load, and so at variable efficiency level. This bond is expressed in the first two lines of (1), because minimization of masses must take in count how much power is to be supply by FC in the second relation, considering that required FC maximum power is related trough inverse function at its efficiency and usury, because it means requiring at FC fast response and transient at non optimal efficiency.

The choice of sizing FC, and thus battery, for power duty is strictly related to the cycle target. In fact if it is considered the example of a continuous urban cycle, the system duty has to supply sporadic peak power, sometime for a long time. This working way would be heavy and harmful for the cell in efficiency terms and also for degrading reasons. So in this case could be suitable reducing M_{FC} or "even" substitute the second line of (1) with the following:

$$P_V \leq P_H = p_{batt} M_{batt}$$

that is an extreme measure for the problem just shown. According to the last consideration it would be useful including in minimization line of (1) the following analytical relation:

$$M_{FC} = f(C, \eta_{FC,} d)$$

that expresses inverse relation of M_{FC} with FC efficiency η_{FC} and durability d, and its dependence by the considered cycle C.

In extreme cases, like the urban cycle just shown, it could be provided the presence of ultra capacitors with the only duty of supplying peak power for short time, so that Fuel Cell can be preserved from excessive and sudden load.

CHAPTER II – FUEL CELL TECHNOLOGY

Proton Exchange Membrane (PEM) Fuel Cell structure and electrochemical process

In order to characterize the FC electrical behaviour, the steady-state and dynamic analysis have been performed.

The use of FC in electrical applications needs an understanding of internal effects for an efficient control of the system as well as to design the storage device, which the FC is equipped with.

The physical effects in the FC sources are various and the analysis needs an interdisciplinary approach. Transport phenomena of mass, energy, momentum and electrical charges play a significant rule in Proton Exchange Membrane Fuel Cells (PEMFC). In this study, the transport and balance equations are the basis of a simulation model, which allows to evaluate the distribution of the physico-chemical parameters, within the structure of a PEMFC reactor. Model validation is presented, with particular attention to critical operating conditions.

PEMFC takes the name from the special plastic membrane used as electrolyte. It is a perfluorinated sulfonic membrane, characterized by an high proton conductibility. The basic cell, which is usually indicated as Membrane Electrode Assembly (*MEA*), combines in a thin structure, no thicker than a few hundred of μm, the electrodes (*anode* and *cathode*) and electrolyte. The electrodes are made of platinum particles which are deposited within a carbon support on the membrane surface. They consist of an

electrically conducting gas diffusion substrate and a porous catalyst layer containing a noble catalyst (i.e. Pt), fig.2.1

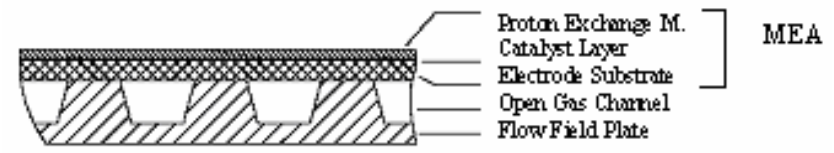

Fig. 2.1 Cell basic structure

The diffusion layers ensure the gas supply for the catalyst sites over the whole active area. These layers are characterized by the porosity and the tortuosity of the material. The diffusion coefficient depends on the properties of the gas diffusion layer of the electrode. The substrate material (normally carbon fiber papers) is used as a spacer to allow the access of the gas even to the catalyst; the catalyst is able to increase the chemical reaction speed and decrease the reagent activation energy.

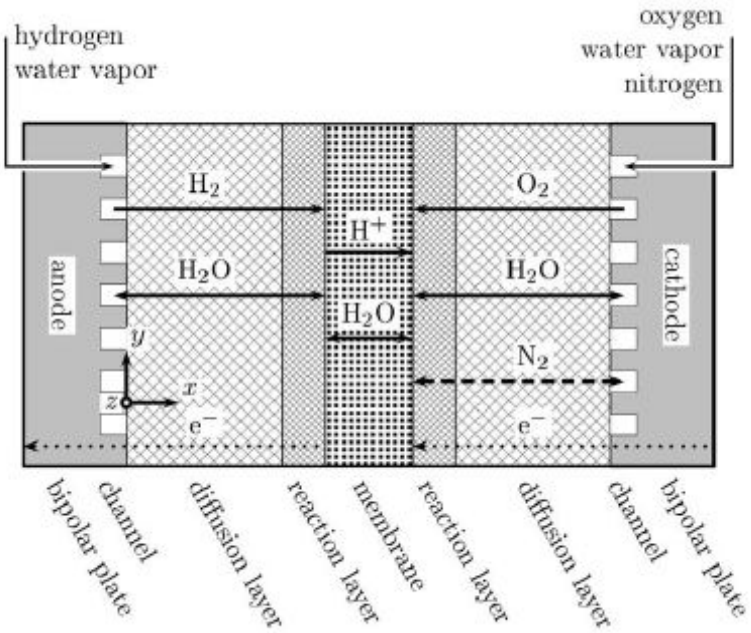

Fig. 2.2. Cross-section of Fuel Cell Structure

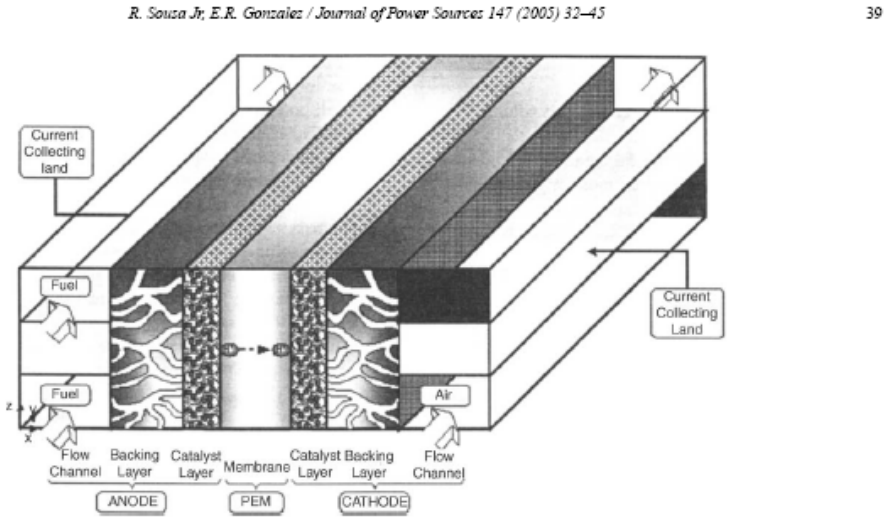

Fig. 2.3 - Three-dimensional figure of Fuel Cell Structure

The electrodes are in contact with the polymer electrolyte membrane ("Nafion"). It is a thin electronic insulator and gas barrier between the electrodes, allowing fast proton

transport and high current densities. The solid electrolyte, which does not diffuse or evaporate, makes the cell able to intermittent operation and rapid load change. As a result of membrane porosity, the particles are introduced into the membrane material. In the membrane two types of transport phenomena exist for the transport of two molecules: water and protons. In the presence of water the sulfonic groups easily dissociate into SO_3^- (fixed charge) and H^+ (mobile charge), and thus the protons encounter a low resistance in moving across a potential gradient. Proton transport depends directly on the current density, while water molecules surround every proton and are dragged with it in the direction of proton flow from the anode to the cathode. This is expressed by a drag coefficient which depends on the humidity of the membrane. A humidity gradient leads to diffusion of water from zones with high water content to zones with low water content. Normally, due to water production at the cathode side, water diffuses from the cathode to the anode side of the membrane, and it is taken in account by a diffusion coefficient. The conductivity depends strongly on the humidity of the membrane. The Nafion membrane thickness varies from 0 to 200 μm [6]. For the reaction, a small water film is necessary to ensure proton transport in the membrane while too much water can constrict the pores so that gas supply is not sufficient any more. Its conductivity is strongly dependent on the level of hydration. The effect of too much or not enough water in the electrode, which modifies the thickness of the water layer, can be observed in FC performances. When it is subjected to temperatures above 100 °C at atmospheric pressure, the conductivity decreases significantly due to dehydration: so the operating temperature is usually limited under

100 °C. The MEA is the PEM core, able to generate electric power at about 1.2 V, with a power density of up to about 1÷1.5 W/cm².

MEA is located between two plates ("Flow Field Plate"). These are usually made of graphite, which channels used to provide the reagents to the electrodes are into. The plate has high electronic and thermal conductivity; it is stable in the operating chemical environment. The thickness is usually of several *mm*, allowing the engraving of the flow channels. The design of the channels influences on the internal water management.

In order to assemble a stack, constituted by a sequence of cells, the plates present flow fields on the right and left sides, supplying gasses to cathode for one side and to anode for the other (so that, they are usually called "bipolar plates"). Stack components include also cooling elements, current collector, and humidifiers. The cooling maintains the thermal operating conditions, whereas the humidifier hydrates the membrane hydration, to increase the proton conductivity.

There are two electrochemical reactions, which occur in a PEM fuelled by hydrogen and oxygen, one at the anode and one at the cathode. The break down of hydrogen into hydrogen ions and electrons occurs at the anode:

$$H_2 \rightarrow 2H^+ + 2e^-,\ E = 0 \quad on\ anode$$

The reaction at the cathode combines oxygen, hydrogen ions, and electrons to form water:

$$1/2O_2 + 2H^+ + 2e^- \rightarrow H_2O,\ E = 1.23V \quad on\ cathode$$

The electrochemical reactions take place at the anode and cathode catalyst layer. At the anode, the gas diffusion layer allows hydrogen to reach the reactive zone, where the

protons cross to the membrane and the electrons goes to the current collector, fig.3; at the cathode, water is formed. The membrane acts as a conductor, able to transfer only the ions H^+ to the cathode.

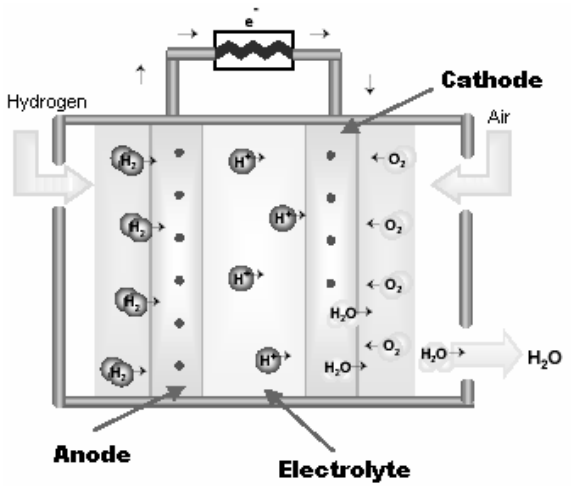

Fig. 2.4 - PEM FC basic operation

Stack dimensions depend on the number of cells, active area, and materials. Power density higher than 1 kW/Kg and 1.5 kW/lt are reached by well designed stack with volume and weight lower than 10 lt/m² and 10 kg/m² respectively.

PEM Local Kinetics

The model of the local kinetics aims at evaluating the reaction rate (i.e. electrical current density) as a function of the driving forces (i.e. electrical voltage and reactant concentrations), at each point on the cell plane.

Actually, in PEMFCs the open-circuit voltage does not correspond exactly to the literature theoretical value expected, Nernst voltage [12], due to parasitic phenomena such as the cross-over of the reactants through the electrolytic membrane and the occurrence of undesirable electro-chemical reactions at the cathode (Costamagna& Srinivasan, 2000).

Although a numerical model is useful for investigating stack parameters the effort required to develop a model can be considerable. This is due to the complexity of the physical processes that occur in the MEA during stack operation including diffusion, electrochemical reactions, capillary action, and electron and ion transfer.

Gas diffusion is the mode of transport for the gases in both anode and the cathode. The fuel diffuses through the anode and oxidant through the cathode. If the process gases are humidified water also diffuses inward through the electrodes. The gases move from the flow channels of the bipolar plate through the porous electrodes to the reaction sites near the membrane. The gases move from and area of greater concentration, the flow channel of the bipolar plate, to an area of lower concentration. They pass into electrode at the rate proportional to the concentration gradient.

As the gases approach to the reaction sites (catalyst locations) they begin to flow via capillary action. In fact, the applications of the catalyst and other materials to the activation layer of the electrodes reduces the size of the passages the gases move

through. As the electrochemical reactions proceed the process gases are consumed and replacement gas diffuses to the reaction sites as the result of the concentration gradient via capillary action.

The ions produced at the anode must be transported across the membrane to the reaction sites in the cathode. The initial force that modes the ions is the positive potential at the anode-membrane interface. This potential results from the build up hydrogen ions at the interface. The force repels the positively charged ions, pushing the outer ions away from the anode. A net drift of ions occurs in the direction of the negative potential. The electrons travel from a reaction site in the anode, through the gas diffusion region of the anode, across the bipolar plate, through the diffusion region of the cathode and finally to the reaction site in the cathode.

CHAPTER III - FUEL CELL MODEL

CHAPTER III - PEM FUEL CELL MODEL

Fuel Cell theoretical model

Interest on fuel cell application moved, and moves, today scientific literature towards research of a steady state electrical equivalent circuit, taking in account physical and operative parameter. This study have to consider also electric element related to alternate current, because the most application are included in this field.

The equivalent complete circuit is made of: reversible voltage, equivalent resistances, equivalent capacitance, equivalents inductances, distributed elements, Warburg elements.

Reversible voltage

For the PEM Fuel Cells the electrochemical equivalent impedance [12] is composed in first place from the thermodynamic potential that represent its reversible voltage E_{Nernst}:

$$E_{Nernst}=1.229-0.85\ 10^{-3}(T-298.15)+4.31\ 10^{-5}\ T\ [\ln(P_{H_2})+1/2\ \ln(P_{O_2})]$$

Equivalent Resistances

As resistive behaviour in PEMFC there is an equivalent contact resistance to electron conduction, R_C, while R_M is the membrane resistance that is represented by the usual form:

$$R_M=\rho_M\, d\,/\,A$$

Where [12]:

$$\rho_M=\{181.6[1+0.03(i_{FC}/A)+0.062(T/303)^2(i_{FC}/A)^{2.5}]\ \}/[\psi-0.634-3(i_{FC}/A)]\exp[4.18(T-303)/T]$$

Where d and A are respectively membrane distance and area.

These two resistances have to be summed, defining so the ohmic resistance:

$$R_\Omega = R_C + R_M$$

Giving the following ohmic Voltage drop:

$$V_\Omega = i_{FC} (R_C + R_M)$$

An other type of resistance has origin from activation of anode and cathode, and so it is expressed through the activation voltage drop:

$$V_{act} = -[\xi_1 + \xi_2 T + \xi_3 T \ln(co_2) + \xi_4 T \ln(i_{FC})] \qquad (1)$$

Where ξ_i are parametric coefficients for each cell model, and T is absolute temperature.

Another voltage drop, coming from the decrease in concentration of oxygen and hydrogen, is concentration voltage V_{con}:

$$V_{con} = -B \ln (1 - J / J_{max}) \qquad (2)$$

Where $B(V)$ is a constant depending of cell type and state, while J and J_{max} are respectively density and maximum density of current.

Equivalent capacitance

The reactive part of the fuel cell is mainly characterized from equivalents capacitance having origin from various phenomena that interest the cells. Among these ones the equivalent capacitance coming from the double layer formed from the electrolyte and the electrode [13], C_{dl}, is predominant. It is defined as partial derivative of load density

on electrodes, regard potential, for fixed values of temperature, pressure and chemical potential:

$$C_{dl} = (\partial \sigma_E / \partial E)_{T,p,\mu}$$

Analogous an equivalent capacitance is defined between the electrodes, that is similar to that one of the classics capacitor, and is therefore function of the dielectric constants of empty and the interposed material (the electrolyte), and of the mutual distance from the plates. Such capacitance defined "geometric" (bulk) is represented from the formula:

$$C_G = \varepsilon_0 \varepsilon_r / d$$

Equivalents Inductances

The inductive [13] part that characterizes a fuel cell is exclusively that one linked to the cable second the classic formula:

$$Z_L = i\omega L$$

and it is therefore a little influential element.

Distributed elements

The combination of the active and reactive impedances just discussed could not be sufficient, in some cases, to the complete description of the cell circuit equivalent, so it is necessary turning to distributed elements, that introduce various values of impedances (resistances, capacitance and inductances) inside the model of the cell and are able to get better the correspondence between the determined circuit and variable frequencies measures obtained on the system.

It is not always possible to determine the cause that generates the presence of these particular values of impedances, for which the distributed elements stretch to represent just the tolerance and ignorance parameters of the system. They take in count phenomena that generate also substantial gap between the mathematical model and the real one, and that are difficultly expectable in analytic way.

Of such elements, the Warburg impedance is the spreader one.

Warburg Elements

The Warburg elements are physically justified as electrodes diffusion, and they are expressed by the following extensive formula [13]:

$$Z_{W,a} = \sigma_a (i\,\omega)^{-1/2} = \sigma_a / [\omega^{1/2}(1+i)]$$

in which σ_a is defined Warburg parameter and function of the reaction rate, concentration and diffusivity of the species *a*, current density and potential. This type of impedance is expressible also in reduced formula (STWE) through the following model:

$$Z_{Wst} = R_W \tanh [(i\,T_W\,\omega)^{\phi}] / (i\,T_W\,\omega)^{\phi} \qquad (3)$$

in which R_W is a Warburg parameter, ϕ is a phase parameter, while term T_W is defined like follows:

$$T_W = \delta^2 / D_a$$

Where D_a is diffusivity of species *a*.

On the basis of aforesaid parameters, the topologies of equivalents circuits have been determined and they are the most spreaded in actual literature:

Randles and Warburg, reported in the following Fig.3.1 and 3.2.

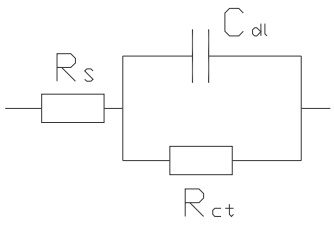

Fig.3.1 – Randles equivalent Impedance

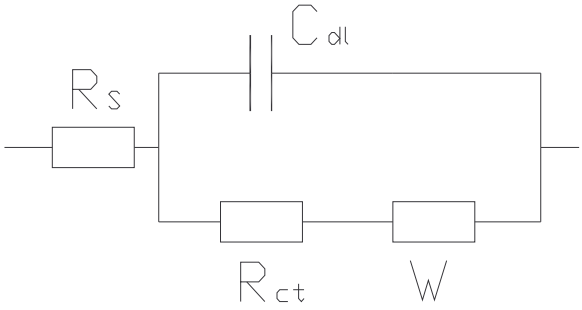

Fig.3.2 – Warburg equivalent Impedance

The difference between this two configuration will be examined in chapter 2, where different operative condition will be considered.

Virtual system implementation of Fuel Cell working with a conversion cluster

In order to make fuel cell automotive or general application achievable, it is very important to analyze and improve the cells behaviour in coupling with other device with

which it is destined to work. Moreover, success of hybrid system is strictly linked to optimization of the operating way, that is to fuel cell steady state operation. This result can be reached just by a complete knowledge of the behaviour system and its electrical equivalent working, that is deduced by static and dynamic application like EIS method, described in chapter IV.

In most spreaded engineering application, fuel cell woks in couple with a conversion system composed by a chopper and an inverter (Fig. 3.3), in order to make energy in the most useful way, but it compels the cells to work at a particular dynamic steady state at which it isn't so easy to determine equivalent circuit, and so its instantaneous and reliability behaviour and performances.

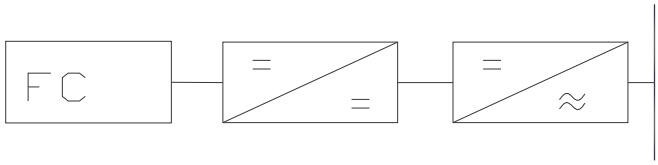

Fig.3.3 – Conventional fuel cell working in couple with conversion system

To taking in account this operative steady state, it is necessary to consider both direct and alternate current electric element, but difficult states in cleaving these two different phenomena.

By adopting mathematical model mentioned in chapter 2, it is possible tracking a virtual polarization curve, typical of a fuel cell working in DC, obtained by considering typical value for each element, taken from [12], reported in Tab. 3.1.

Param	**Value**	**Param**	**Value**
n	32	ξ_1	-0.948
A	64 cm^2	ξ_2	0.00354
d	178 μm	ξ_3	$7.6\ 10^{-5}$
T	333 K	ξ_4	$-1.93\ 10^{-4}$
P_{O_2}	1 atm	ψ	23
P_{H_2}	0.2095 atm	J_{max}	0.469 A/ cm^2
R_c	0.0003 Ω	C	3 F
B	0.016 V		

Tab. 3.1 – Typical values of fuel cell elements

By assuming the value reported in tab. 3.1, a simulation in Matlab was execute, by growing current step by step, till to obtaining a complete graphic, Fig 3.4.

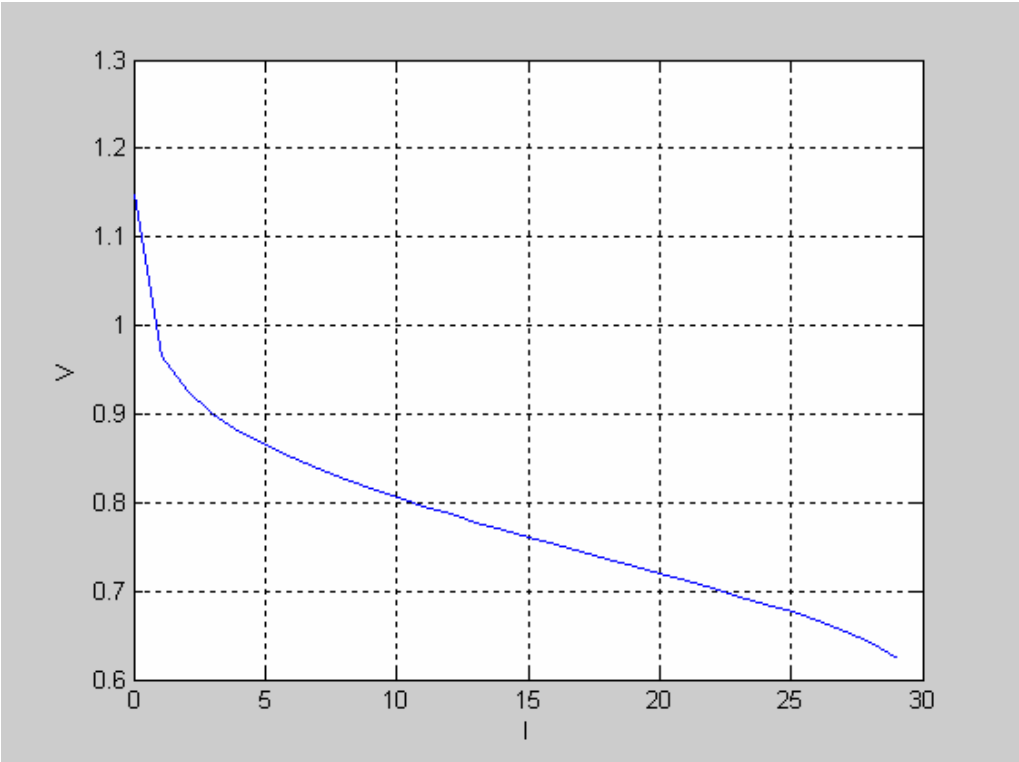

Fig. 3.4 – Polarization Curve related to Tab 3.1

Fig. Y, like all fuel cell polarization curve, manifest a large middle linear range, where it is possible to use overlap of effect, that is considered separately DC and AC current.

For AC component it would have been very difficult to examine the equivalent system, because of its irregular wave shape (Fig 3.5) , so it has been necessary to adopt the (*good*) approximation to the fundamental harmonic. Such approximation results in a a satisfactory approximation, as in many conversion system applications. These hypothesis make possible the transformation of Fig 3.5 into Fig. 3.6, and implementation of Fig. 3.7, that are results of Matlab simulation early mentioned.

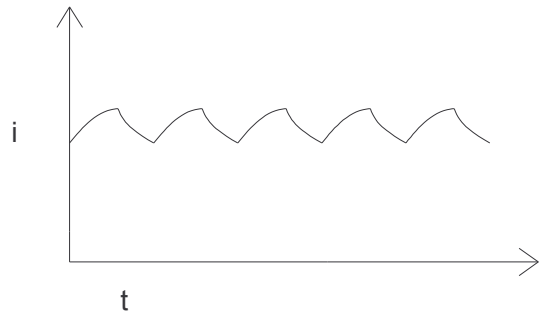

Fig 3.5 – Typical wave shape of converter applied to fuel cell source

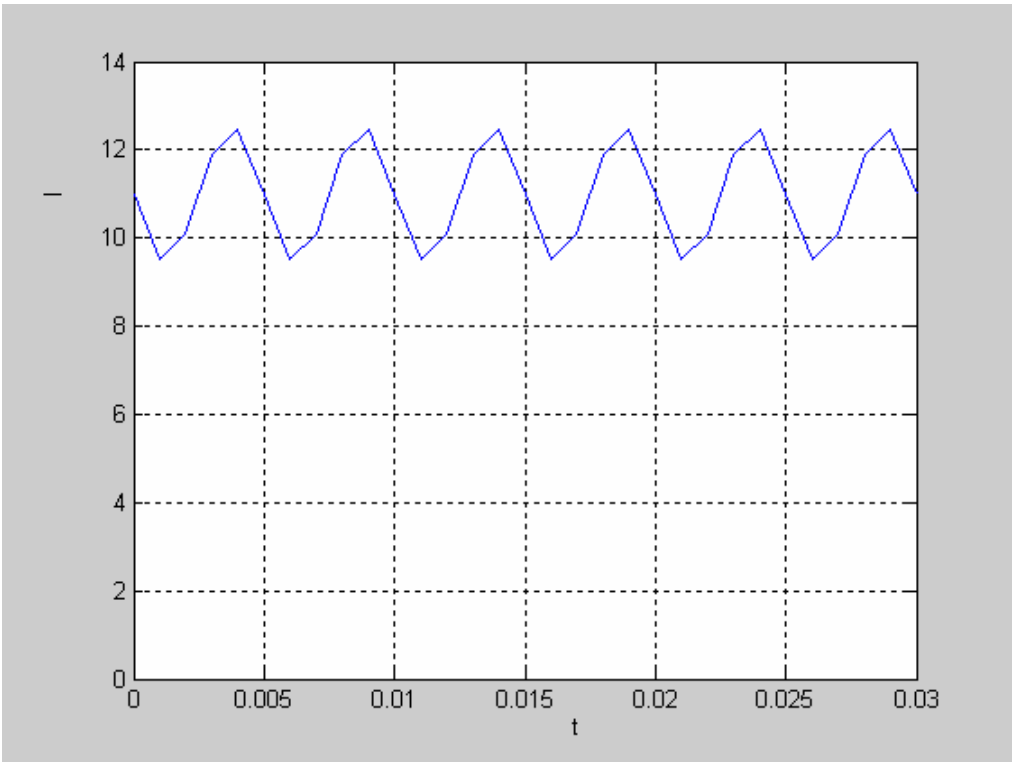

Fig. 3.6 – fuel cell current vs time

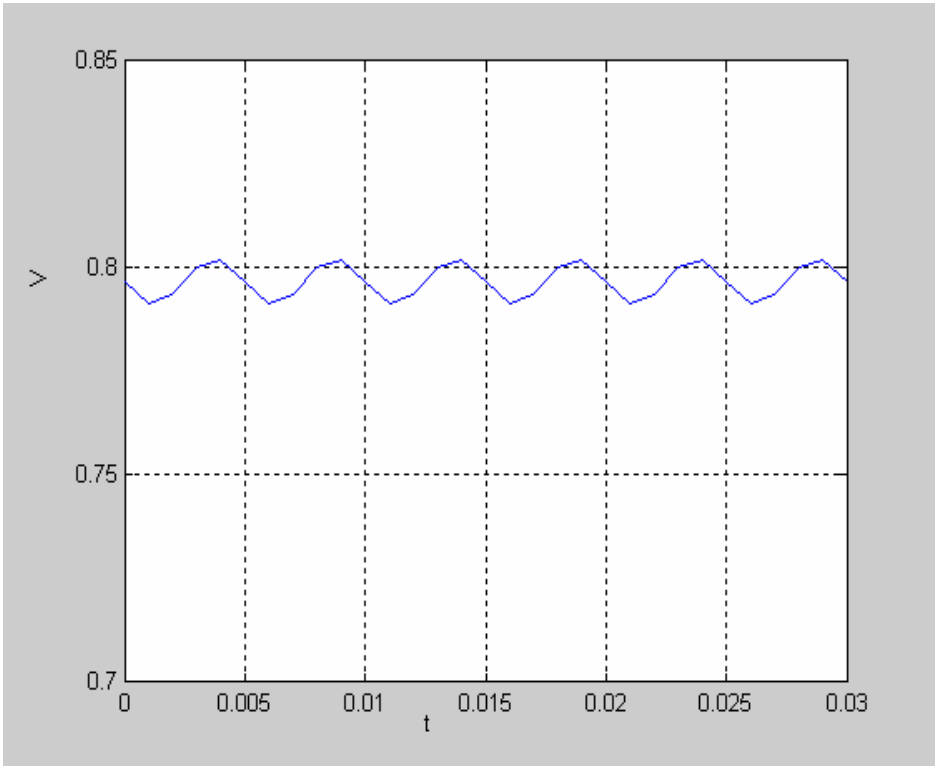

Fig. 3.7 – fuel cell voltage vs time

Assuming these hypothesis, that is overlap effects and sinusoidal voltage and current for AC component, and considering the mathematical model of chapter 2, the classical DC curve polarization of chapter 2 becomes the following curve (Fig. 3.8), where is underlined the range in which voltage-current relation can vary in time domain.

Obviously this rule is true just in linear curve range, because, otherwise, overlap effect rule isn't applicable, and so all theory loses its worthiness .

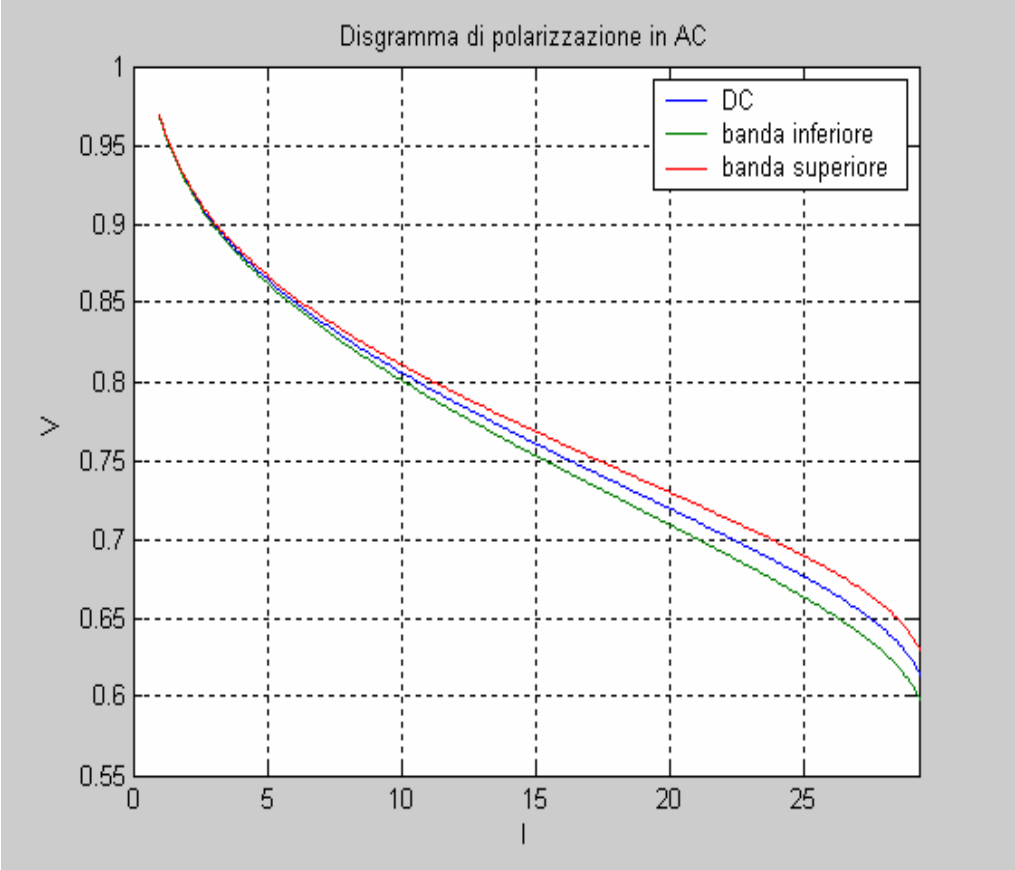

Fig. 3.8 – Polarization curve in matched AC-DC state

In order to obtaining a real, worthiness and complete picture of fuel cell electric operating parameter in overlapped DC-AC state, that is in coupling with a conversion cluster, a three-dimensional figure was implemented where voltage and current are reported versus the time. This application, that has been derived by a simulation routine implemented in Matlab, gives for every fuel cell considered its real time theoretical behaviour, by introducing its own parameters.

Fig. 3.9 is an example of before mentioned simulation by considering for fuel cell parameter the Tab 3.1 (of chapter 3) one.

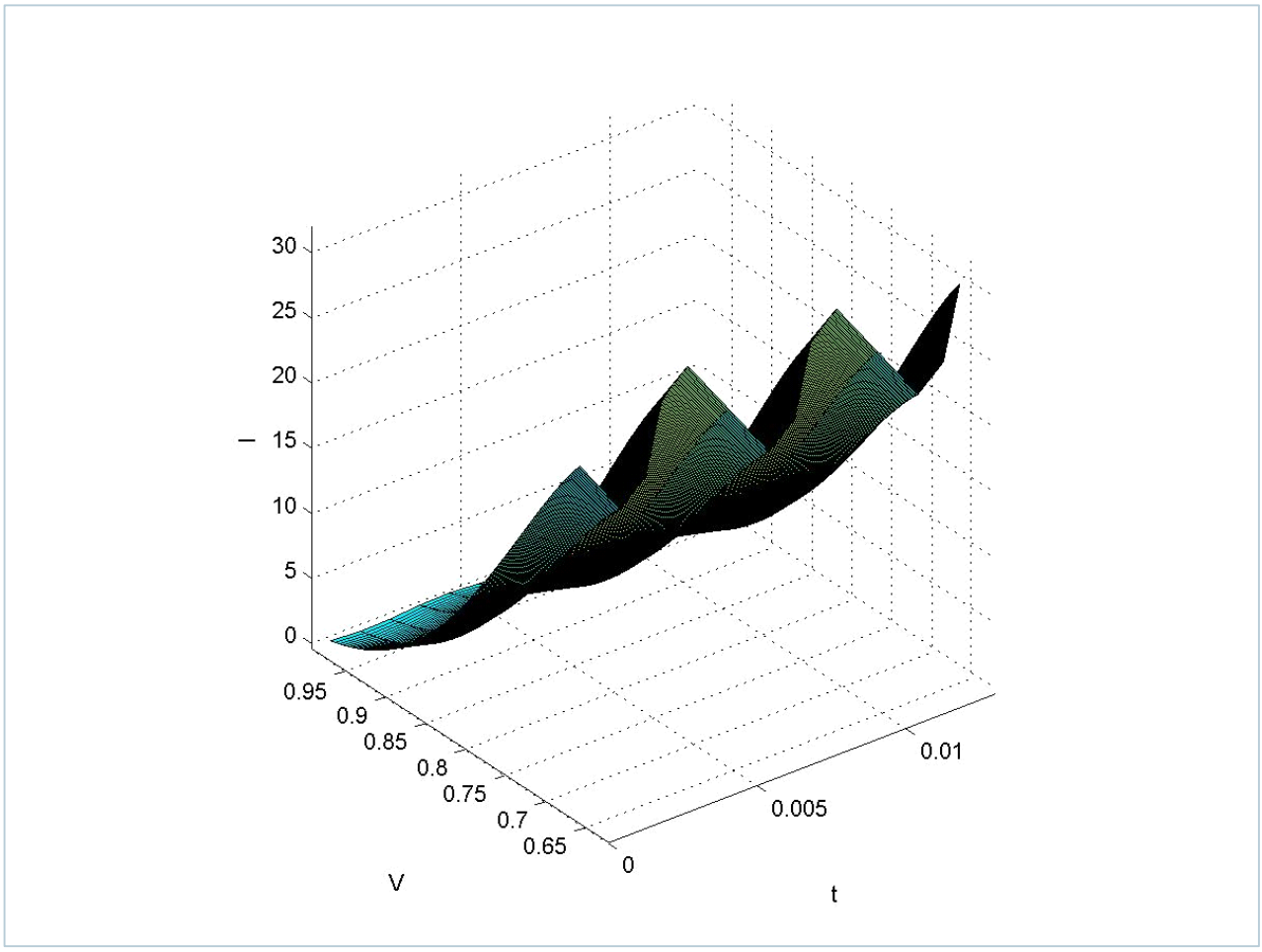

Fig. 3.9 – voltage and current theoretical variation in time domain

CHAPTER IV – ANALYSES AND SIMULATIONS OF THEORETICAL MODEL

CHAPTER IV– ANALYSES AND SIMULATIONS OF THEORETICAL MODEL

Electrochemical impedance spectroscopy (EIS) method

Electrochemical Impedance Spectroscopy (EIS) method is already used in applications of electrochemical storage cells, to individuate the values of the electrochemical system equivalent impedance. It is based on the behaviour that the system gives back to external signal, incoming at various frequencies, making it possible the implementation of a circuital model equivalent to the system. The method is effectively little invasive, so that it doesn't modify the characteristics of the system. The cell is loaded with an alternative signal, with a voltage varying in ±(20÷30) mV peak-peak.

For the implementation of EIS method it is necessary the preliminary study of the electrochemical system under investigation, in order to characterize the hypothetical characteristics of the equivalent circuit. The first step for an application of EIS method consists of identifying the parameters that compose the system in object to which attributing some values [13]. EIS method can concur to fast and effective system diagnostic.

Static analysis and simulation

On the basis of the just mentioned equivalent circuital models a virtual Fuel Cell has been implemented in Matlab, in order to analyze the system and to deduce important observation.

CHAPTER IV– ANALYSES AND SIMULATIONS OF THEORETICAL MODEL

In the simulation the parameter of [12] (Tab. 3.1) have been adopted.

By using the mentioned model and parameter, the polarization curve has been obtained, characterizing the cell. In order to get this graph, a growing DC current has been imposed on the equivalent impedance, giving the graphic of Fig 4.1 .

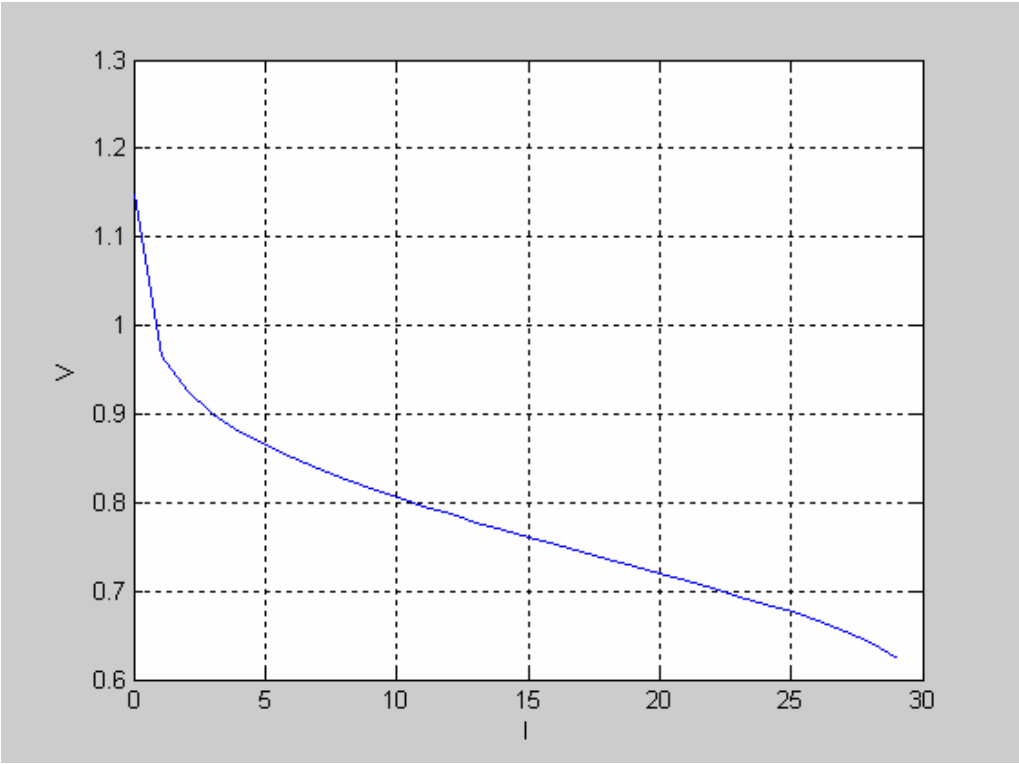

Fig 4.1 - Polarization curve

A lot of simulation in different frequency range, and at various current values, has been implemented on the Randles model.

Dynamic analysis and simulation

In order to provide the answer behaviour of the system, and thus its electroscopic characteristics, the resulting values have been gathered up in Nyquist graphic. From these ones it has been noted that Randles circuit is good to describe just low current answer of fuel cell; in fact growing up current level the diffusion phenomena becomes very influent, so that change frequency response of the system, as it is possible see by comparing real experimental Nyquist diagram [14] and those ones obtaining by aforesaid simulation.

Moreover it is evident like impedance module decrease by current according to polarization curve of Fig 4.2 .

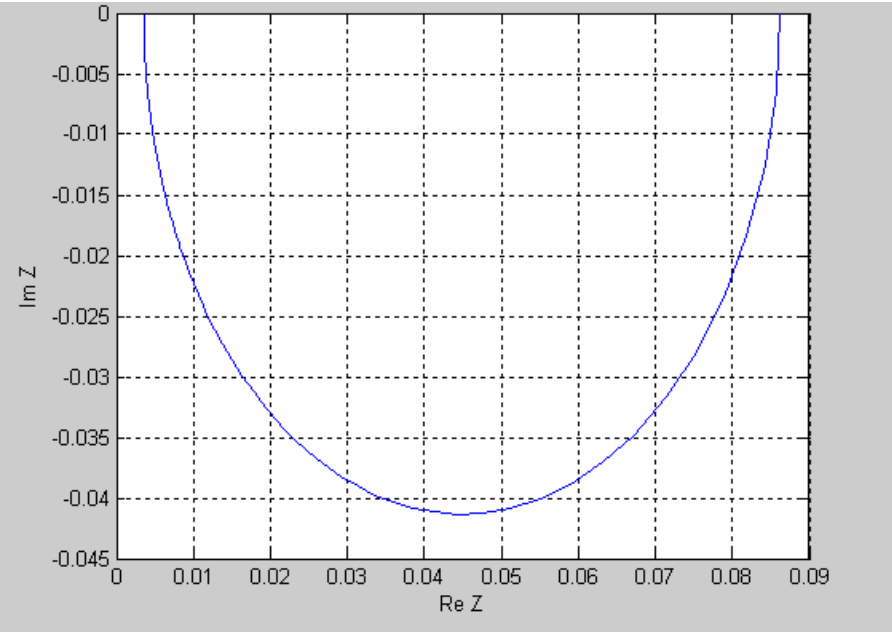

Fig 4.2 - Nyquist diagram of Randles model with I=5A

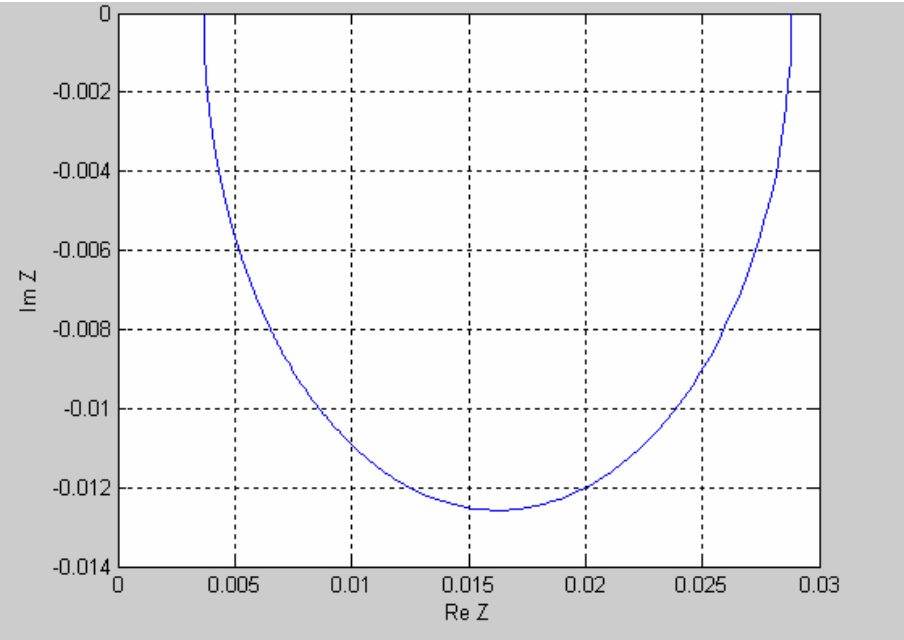

Fig 4.3 - Nyquist diagram of Randles model with I=20A

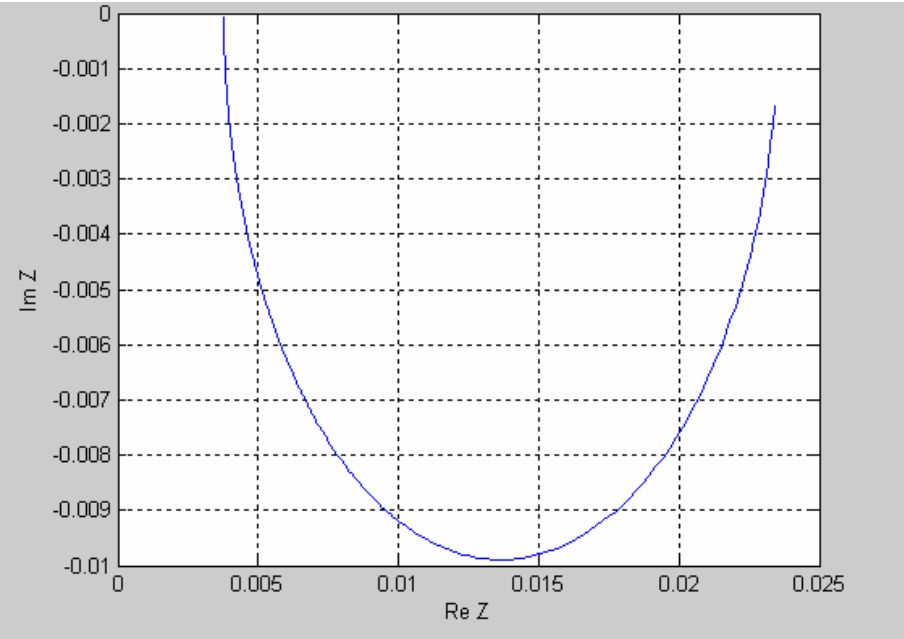

Fig 4.4 - Nyquist diagram of Randles model with I=30A

After these simulation, other ones have been implemented but this time focalized just on a simple distributed model: the Warburg one (Fig. 4.5). Obviously, as defined by the analytical model, Warburg impedance (chapter 3) is current independent, thus its Nyquist diagram remains constant respect to current variations, as Fig. 4.5 shows.

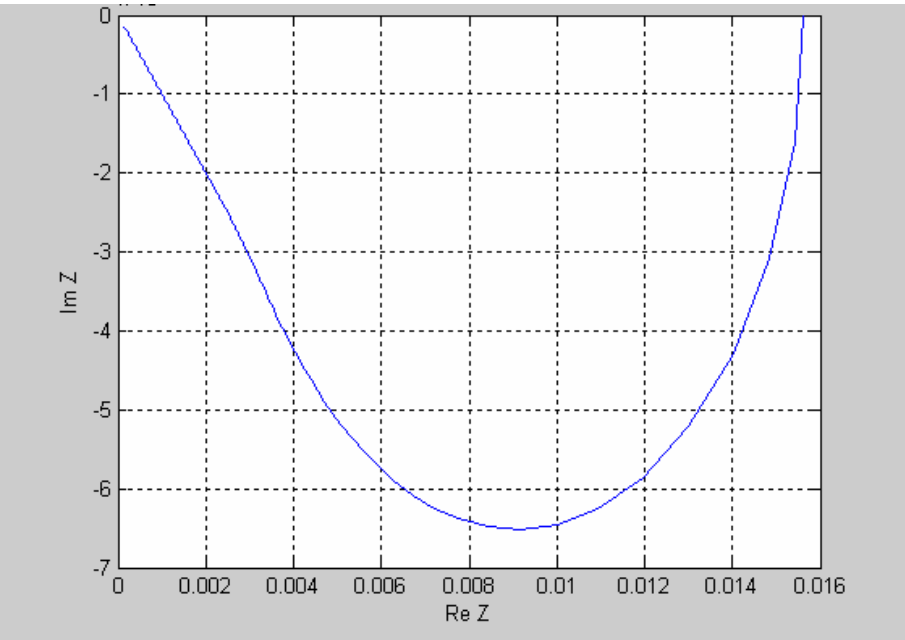

Fig 4.5 - Nyquist diagram of just Warburg impedance with I from 5A to 30A

To ending impedance electroscopic analysis, a complete impedance circuit, composed by Randles circuit and Warburg elements together, has been implemented in simulation, always processed to frequency and current variations (Fig. 4.6).

The Nyquist diagrams, consequent to last simulations, prove as the complete model complies with the real experimental result of [14].

To underline the influence of diffusion and the validity of proposed model are following reported Nyquist graphic by adopting the complete Warburg model,

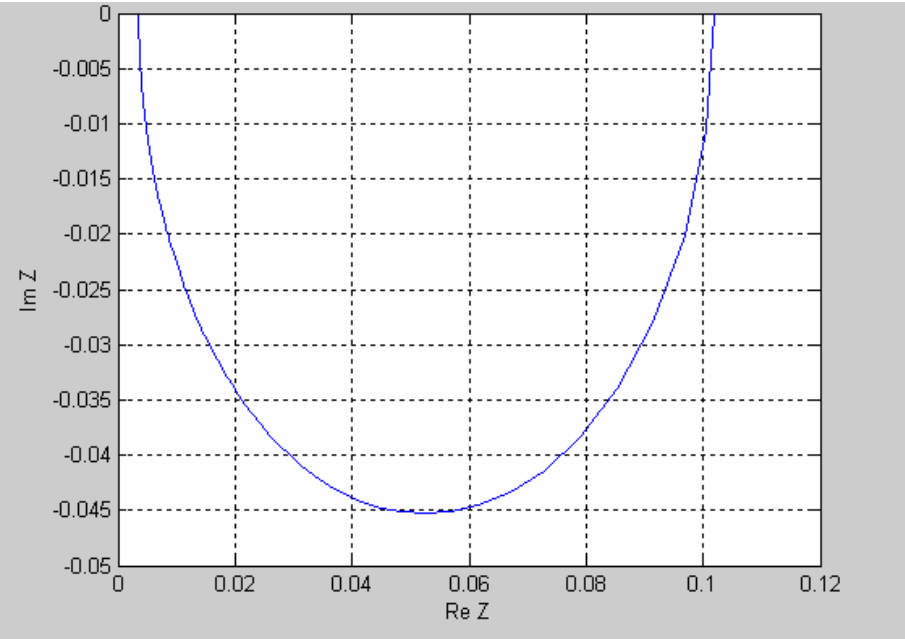

Fig 4.6 - Nyquist diagram of Warburg model with I=5A

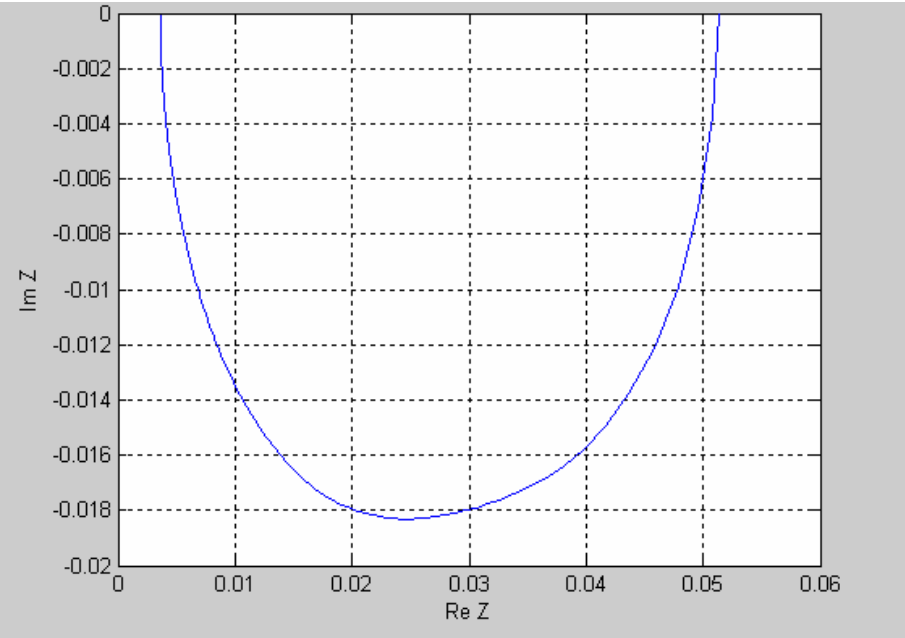

Fig 4.7 - Nyquist diagram of Warburg model with I=15A

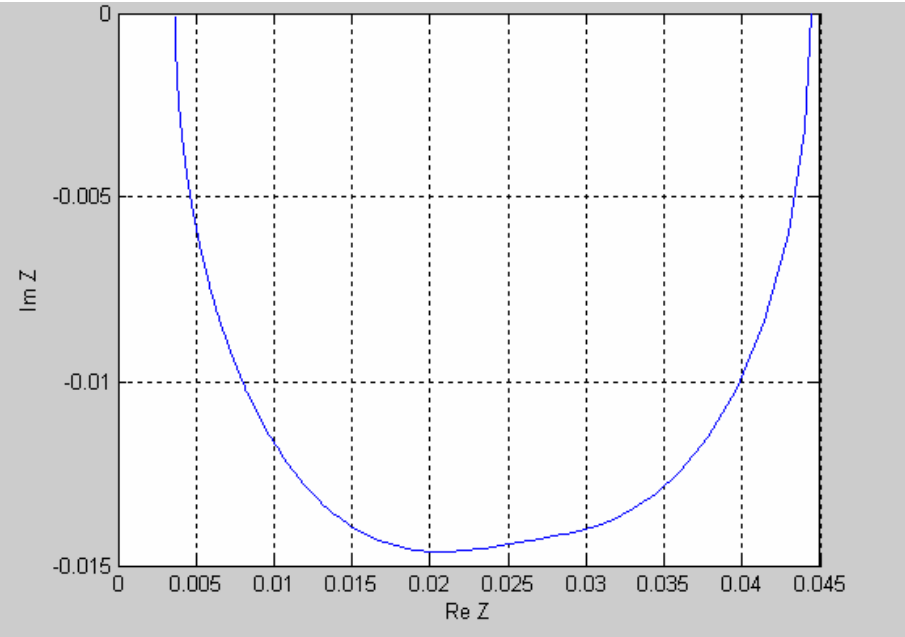

Fig 4.8 - Nyquist diagram of Warburg model with I=20A

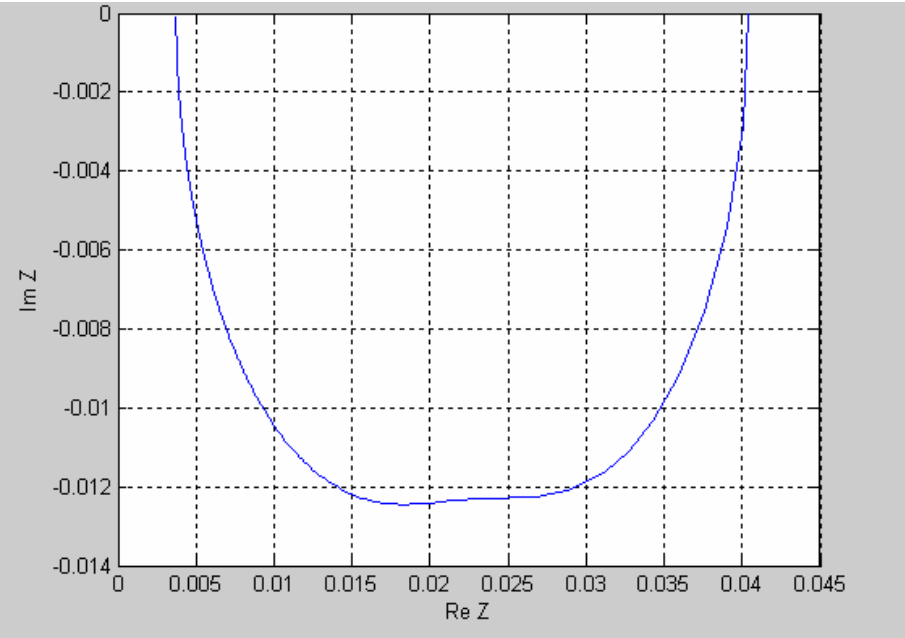

Fig 4.9 - Nyquist diagram of Warburg model with I=25A

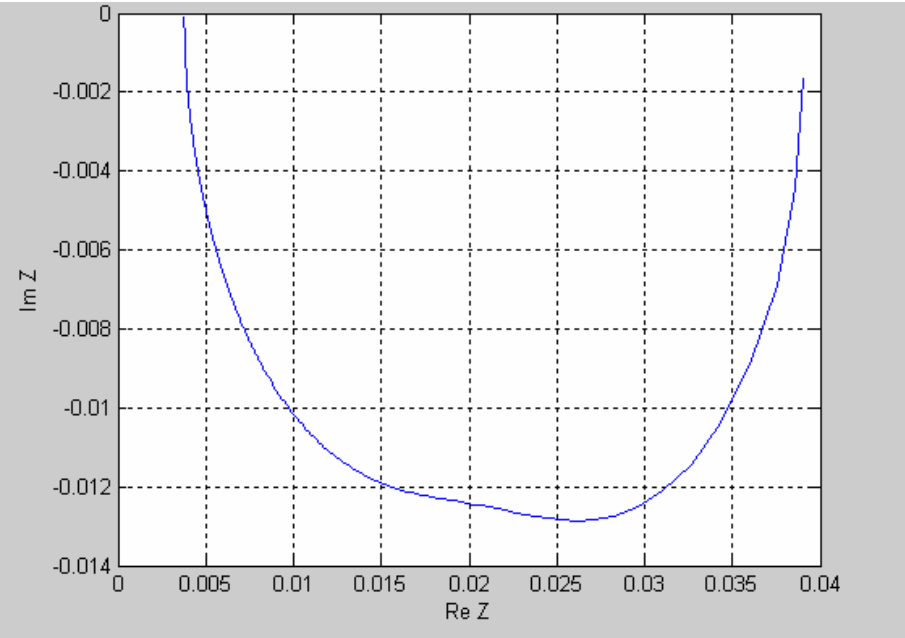

Fig 4.10 - Nyquist diagram of Warburg model with I=30A

At low current level the Fig.4.2 and Fig.4.6 diagrams are very similar, but growing up the current in Warburg model a two time constant model is shown, and the graphic becomes similar to the experimental one spreaded in research journals.

This phenomena can be explained by observing the not evolution of Nyquist diagram at growing current, in fact, as defined the analytical model, Warburg impedance is current independent; on the contrary the other Resistance (1,2 chapter 3) decrease like the polarization curve Fig 3.8 shows, and so it takes a grower weigh in the equivalent impedance, even if it is always present in the model at different intensity.

Main considerations on the theoretical model

The current-voltage curves show a typical PEMFC performance, which is characterised by the presence of three different regions: (i) semi-exponential region, at very low current density, where the cell behaviour is mostly determined by the activation losses at the cathode; (ii) linear region, at intermediate current densities, where the ohmic losses through the membrane play a major role; and (iii) voltage drop, at high current density, due to the mass transport limitations occurring in the electrodes and in the membrane

CHAPTER V - ELECTROCHEMICAL IMPEDANCE SPECTROSCOPY EXPERIMENTAL RESULTS

CHAPTER V - ELECTROCHEMICAL IMPEDANCE SPECTROSCOPY EXPERIMENTAL RESULTS

Hardware and software laboratory

To validate virtual model implemented in Matlab field, a real workstation has been realized in laboratory (Fig. 5.1), assembled in order to conduct the same experiments virtually accomplished.

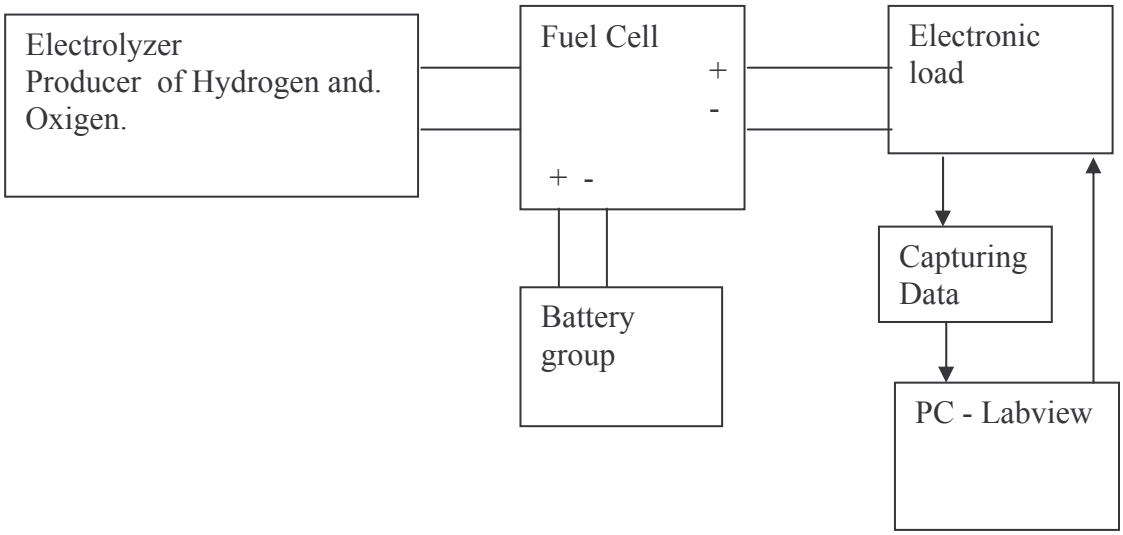

Fig.5.1 – test-bed

This instrumentation is composed by a 1 kW Fuel Cell source, a "Independence 1000" by Reli On (Fig. 5.2) , for the which a four battery group is used as start up system, interfaced by a DC breaker to be opened during cells steady state.

Fig. 5.2 – Fuel Cell tested

In series, placed before the DC fuel cell converter, an electronic load is connected, the "High Power Electronic Load 63202 Series" (Fig 5.3). The last is a passive system that can generate some wave shape at different current, resistance, voltage or power values, thank to transistor commanded by feedback regulator, and it is programmable manually or by remote control.

Fig 5.3 – electronic load

In this way, it is possible obtaining the same condition generated by a conversion utilization system, at various switching frequency range. The Fuel Cell is fed by an electrolyzer grid-connected, that fills a three bar hydrogen tank (Fig. 5.4).

Fig. 5.4 - electrolyzer

All the output measures are recorded by a data capturing interfaced with a personal computer, managed by a software implemented in Labview (Fig. 5.5). All these data are later imported and elaborated in Matlab and Simulink field to obtain table, graphs and data sheet of experimental results.

Fig. 5.5 – capturing system

CHAPTER V - ELECTROCHEMICAL IMPEDANCE SPECTROSCOPY EXPERIMENTAL RESULTS

Main results of static analysis

First target of experimental proofs has been obtaining a static diagram, expressing how voltage changes by varying current, in order to validate theoretical hypothesis about impedance behaviour of cells at different states. It is very important to underline that the stack of fuel cell, used in the experiments, have already worked for a long number of hours, and above all that it is several years old, so that its electrical characteristics have been subject to changes due to age and electrochemical degradation. It is more evident in the first part of polarization curve, precisely in the initial activation one, where the trend follows an unconventional shape, in the which voltage look like not to be greatly influenced by current variation, causing a right shift of the current (X) axis, that is a delay in activation phase. This initial shift influences, obviously, all the curve by shifting right ohmic and concentration current range, so that they show themselves at higher current value. In particular the concentration phenomena is subject to a strong range constriction, because the tested cells have decreased at 70% their nominal power, under the age effects, and so the last gap has been reduced at few Ampere.

The capturing operation has been executed by a current control on the electronic load starting from zero, and increasing by unit step of 1 Ampere.

This proofs, executed by hot start and cold start, have returned about the same results. Also keeping time of every step has been changed from 1 second to 20 second, but no sensible differences have been noticed.

The following table and figures shows the captured value of static analysis.

Step	**1**	**2**	**3**	**4**	**5**	**6**	**7**	**8**	**9**	**10**
V[V]	53	53	53	53	53.2	53.2	53.3	49	46.4	37.8
I[A]	1	2	3	4	5	6	7	8	9	10

Step	**11**	**12**	**13**	**14**	**15**	**16**	**17**	**18**	**19**	**20**
V[V]	35.0	34.1	32.5	29.7	29.5	28.4	27.5	26.8	26.0	24.9
I[A]	11	12	13	14	15	16	17	18	19	20

Step	**21**	**22**	**23**	**24**
V[V]	24.0	23.0	22.1	20.2
I[A]	21	22	23	24

Tab 5.1 – captured data

Ignoring the initial part, for the above mentioned reasons, the polarization curve is the following

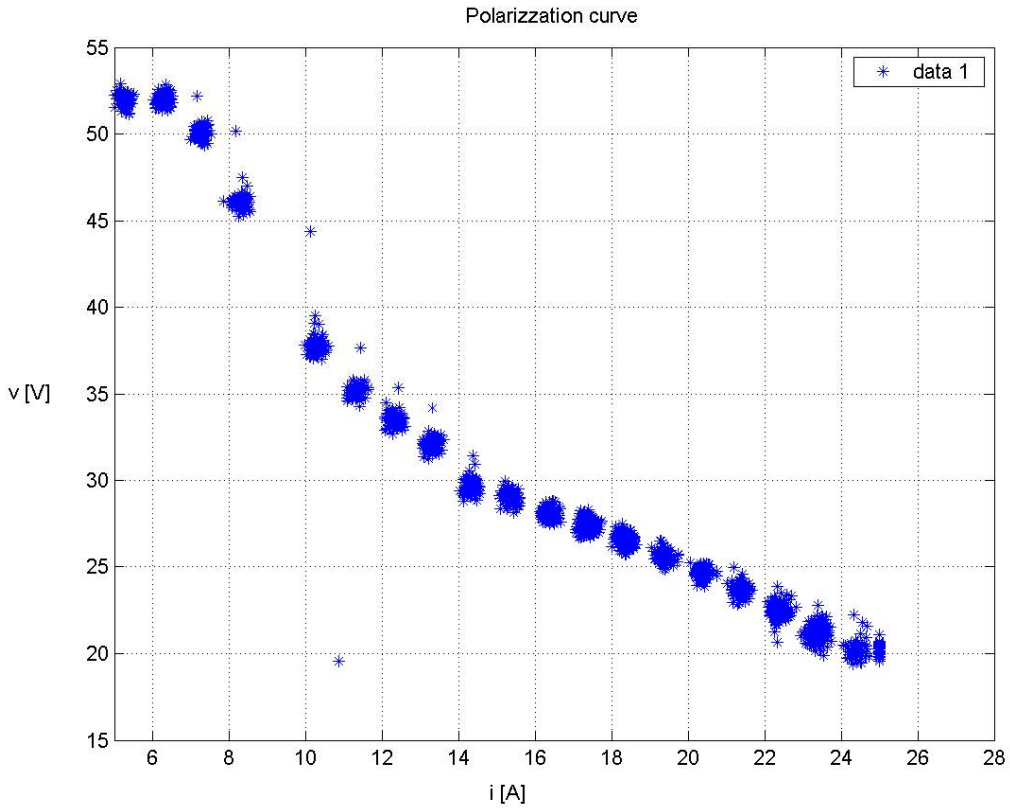

Fig 5.6 – real polarization curve

The graphic has been obtained by sampling many voltage and current values for every step considered, and than it has calculated the average value for every point.

By observing the figure, it is easy to notice that concentration zone is nearly absent, and so it is very important to implement a curve fitting, in order to complete the polarization trend and to interpolate the recorded point value.

A linear interpolation has been leaded on the polarization curve, by considering local constant value of equivalent resistance for activation, Ohmic and concentration zone.

These values have been validated also by results of dynamic proofs, implemented on linear part of polarization curve.

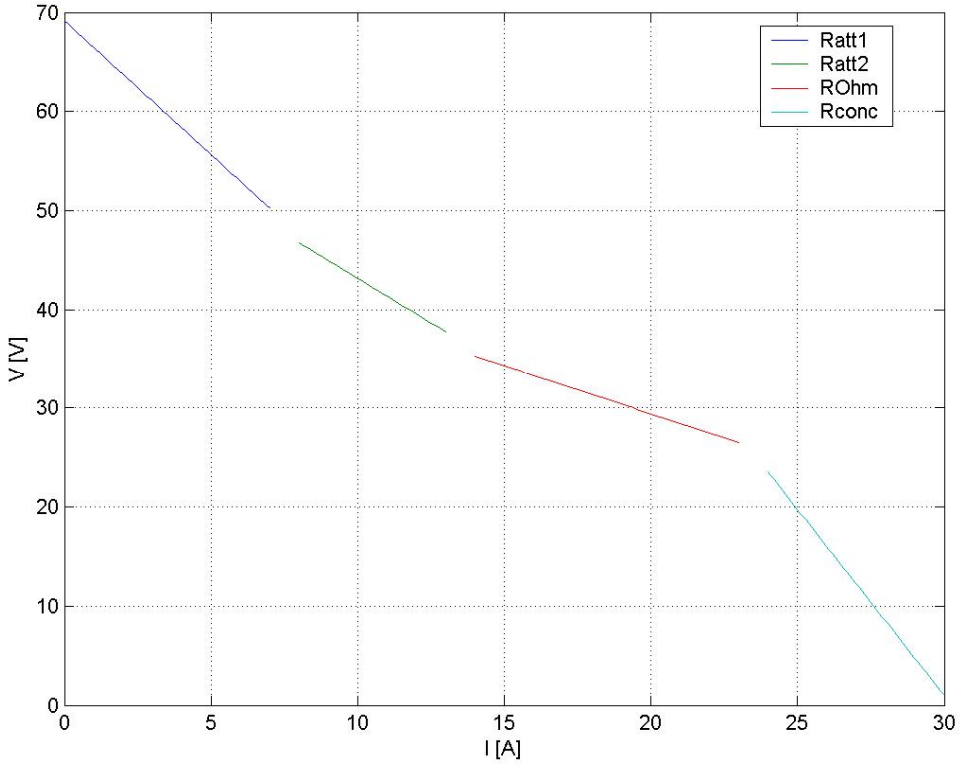

Fig. 5.7 – linear fitted polarization curve

The found equivalent resistance for every part are the following:

R activation in first part = 2,7 Ω;

R activation in second part = 1,8 Ω;

R Ohmic = 0,03 Ω;

R concentration = 3,75 Ω.

The fitting by reduced parameter number, has been due to excessive complexity of whole parameter system iterative method, too hard to be implemented by ordinary personal computer, in ordinary time.

These single values are valid, with little approximation, just in local gap. So, in order to have a single analytical model equation, a mono dimensional polynomial interpolation method has been applied, by evaluating the least square error for every parameter set and degree of polynomial interpolator. Otherwise, in fitting curve, it has been considered the shape that an electrochemical polarization curve must be subject to; for example, negative and growing with current voltage value has been rejected.

Eventually the following 4 degree polynomial expression has been evaluated the best fitting for the fuel cell static characteristic:

$$V = - 0.00069I^4 + 0.04I^3 - 0.75I^2 + 3.2I + 50$$

where V is voltage and I current.

Plotting this equation and overlapping over the experimental one the following figure has been obtaining:

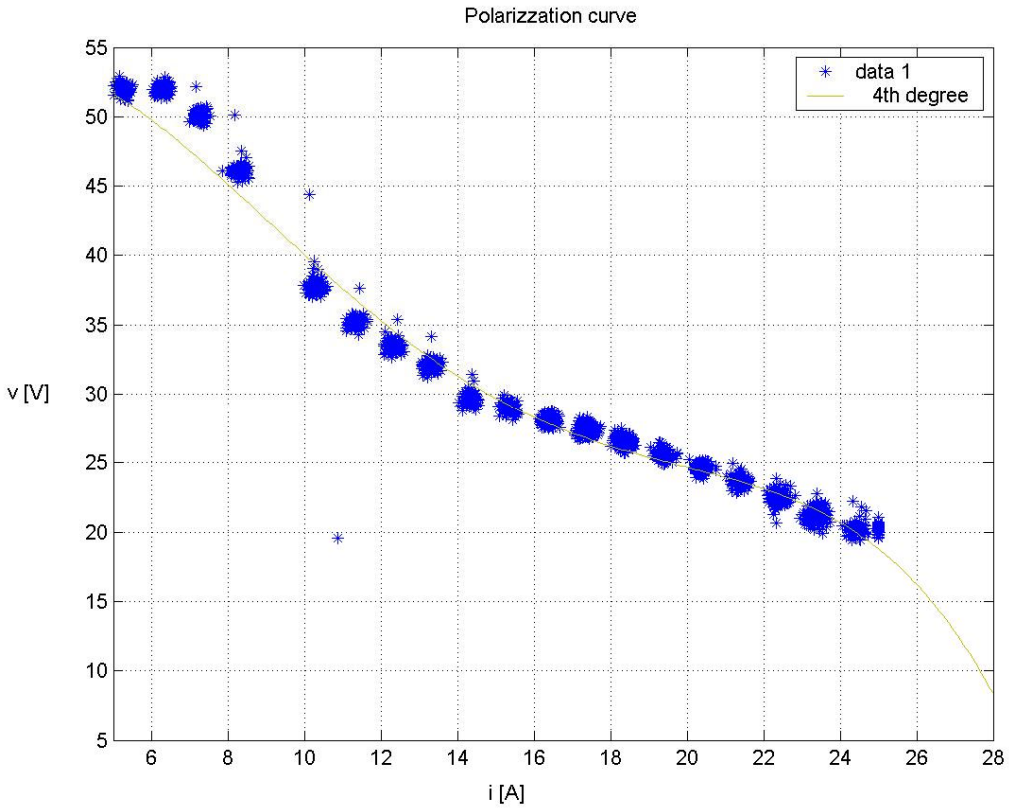

Fig 5.8 – Comparison real and polynomial fitted polarization curve

Dynamic analysis and simulation

Dynamic analysis has been conduced, by considering static one, in order to establish right points and range, where starting hypothesis are respected to apply Electrochemical Impedance Spectroscopy method. In fact, to implement this kind of analysis, the voltage-current point, at which frequency variation is applied, must be included in an enough large linear gap, so that all theory exposed in chapter III and IV can be

validated. So the considered voltage-current value for dynamic analysis are 9,5 A and 16,5 A, around which a 2,5 A ripple has been overlapped.

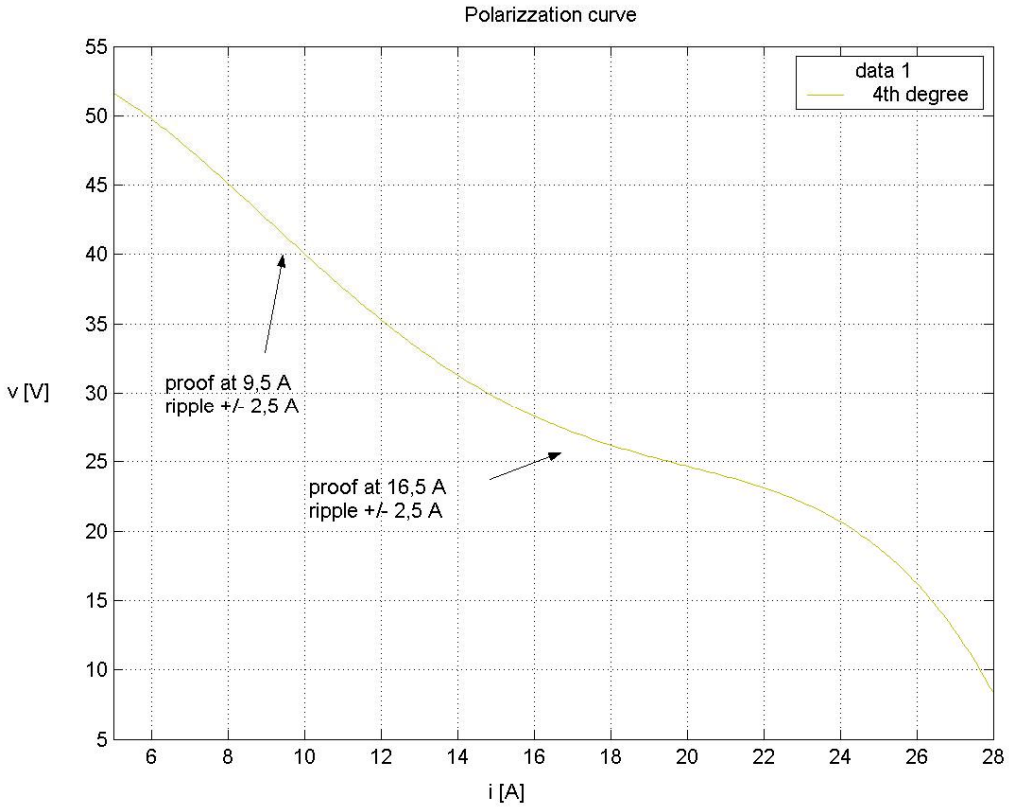

Fig 5.9 - polynomial fitted polarization curve

After fixing work point at 16,5 A, a 2,5 A ripple has been overlapped, that is, a square wave flicking between two current values has been imposed by the electronic load, and these values are 14 A and 19 A.

This setting has produced the following graphic results, in which has been considered as example a 20 Hz frequency:

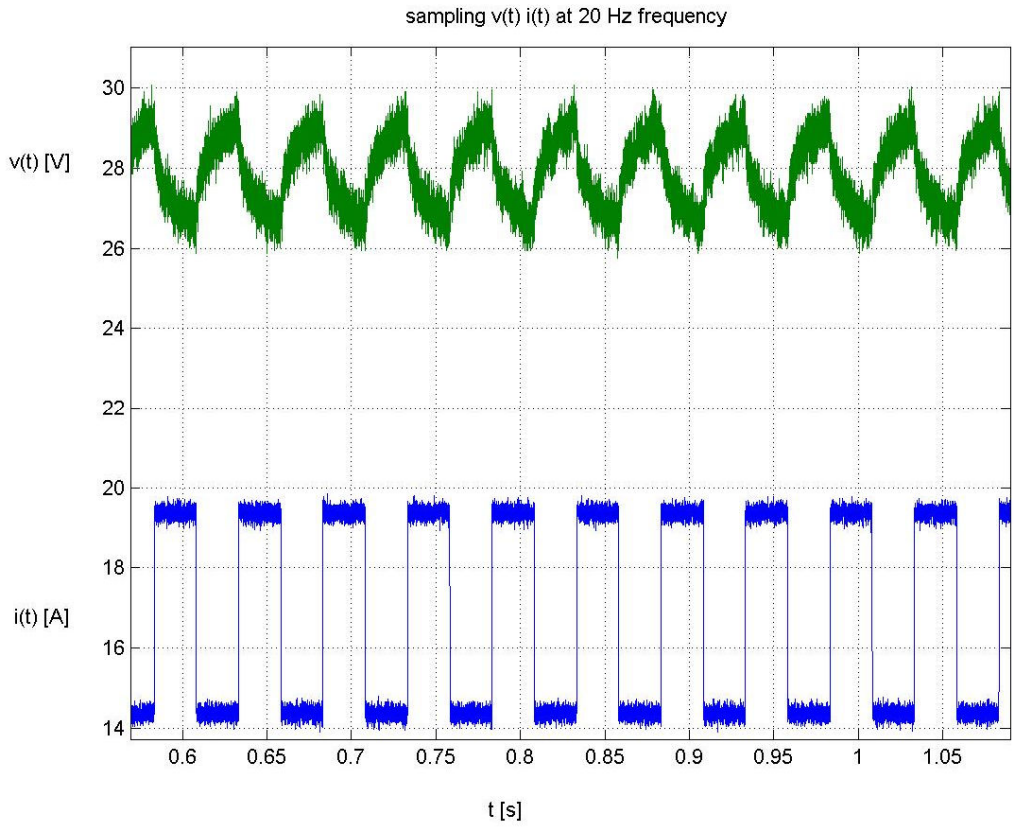

Fig 5.10 – Real time current and voltage at 20 Hz

Obviously, these results in time domain could be not used in analytical elaboration, so instantaneous values has been used to obtain, by Matlab Fourier tool, the fundamental

data of voltage and current, in order to reproduce respective sinusoidal wave in time domain of figure 5.11.

These waves are reported on the zero of voltage-current axis, because they are considered as ripple on a constant voltage or current value.

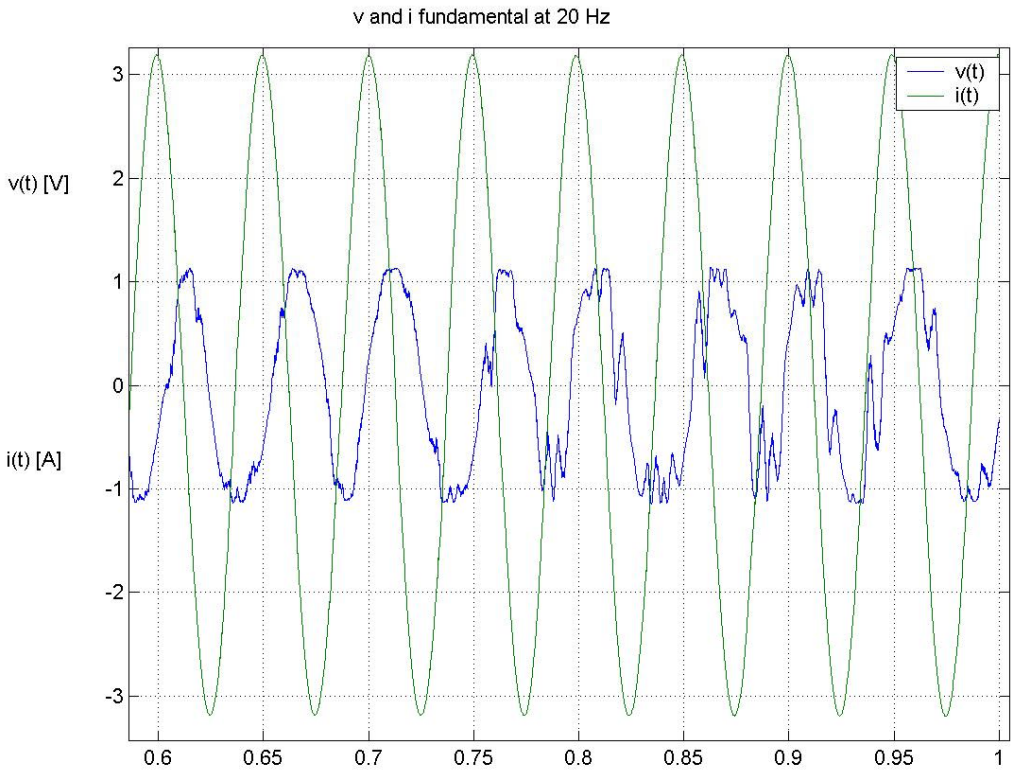

Fig 5.11 – Fundamental current and voltage at 20 Hz

It is clear that noise and measurement errors influences sinusoidal waves, above all the voltage one, whose size get comparable with noise size growing up frequency, in fact fundamental elaboration at 50 Hz is following showed:

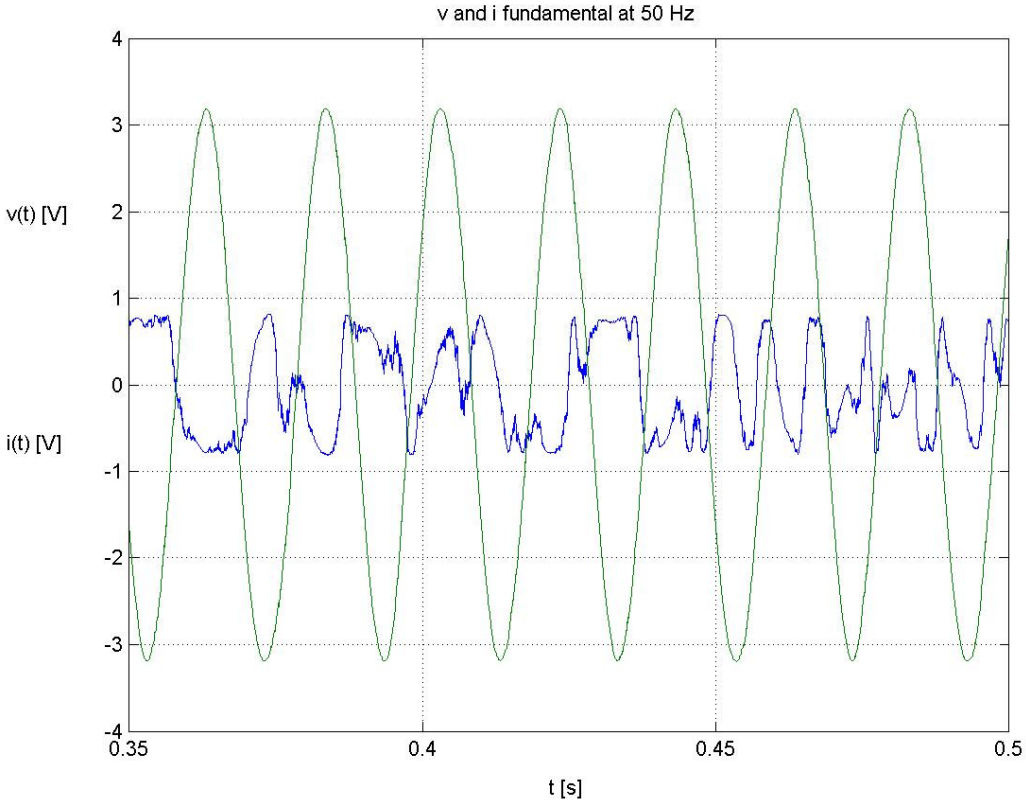

Fig 5.12 – Fundamental current and voltage at 50 Hz

Obviously a such distorted sinusoidal function could be not considered believable in an analytic application, so, to ride over the problem, an average value of Fourier analysis has been calculated. In this way a constant fundamental parameter is considered in graphic, and above all, in theory elaboration.

Last consideration has shown the following results, that is comparison between real and fundamental curve at example frequency of 15 Hz

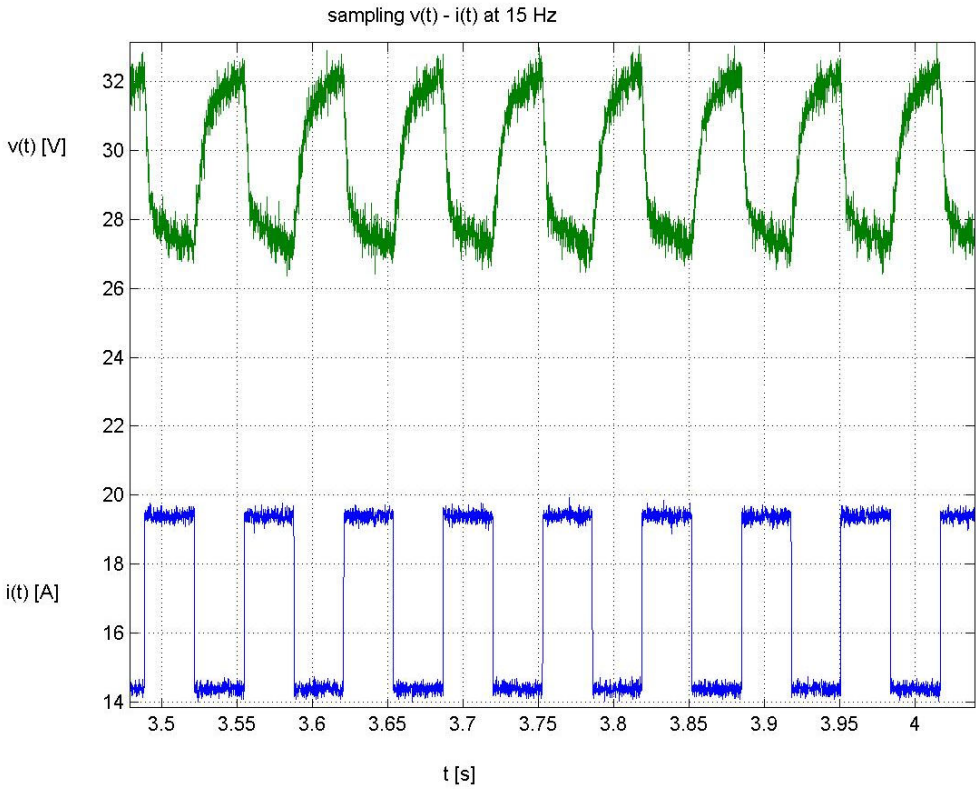

Fig 5.13 –Real time current and voltage at 15 Hz

It is important to notice that voltage wave has classical shape of a capacity load, that is delay of voltage respect to current, visible both in real and fundamental graphic.

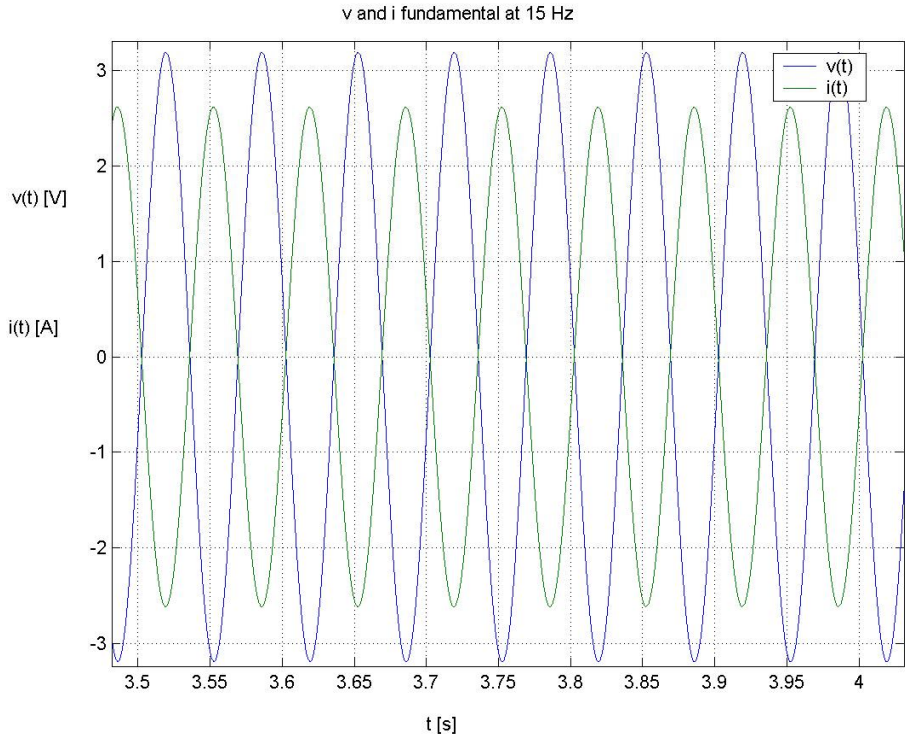

Fig 5.14 – Mean fundamental current and voltage at 15 Hz

Growing up frequency, voltage is filtered and so levelled by capacity originated from cells coupled surfaces. This phenomena decrease very much voltage size, so that it becomes comparable (or smaller) with noise also in real capturing, and so generating uncertain trend, unhelpful to every general model treatment.

For example a 400 Hz frequency capturing is shown.

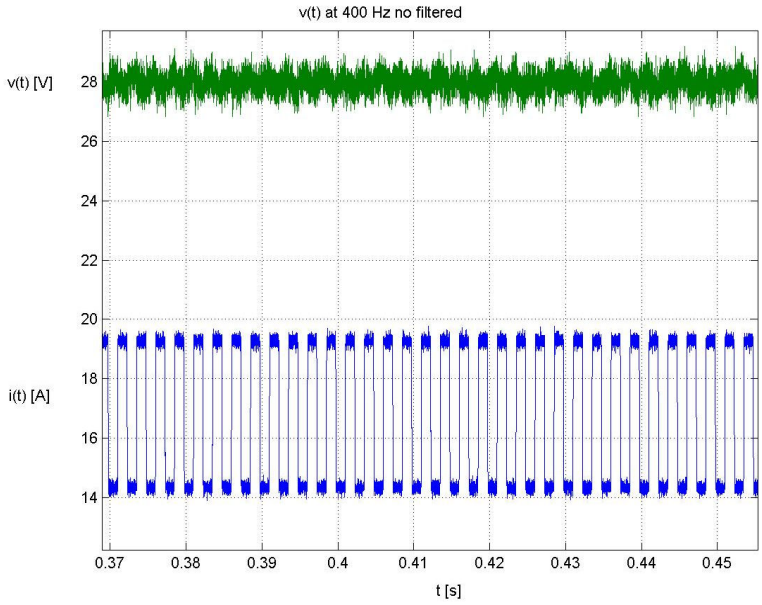

Fig 5.15 – Real time current and voltage at 400 Hz

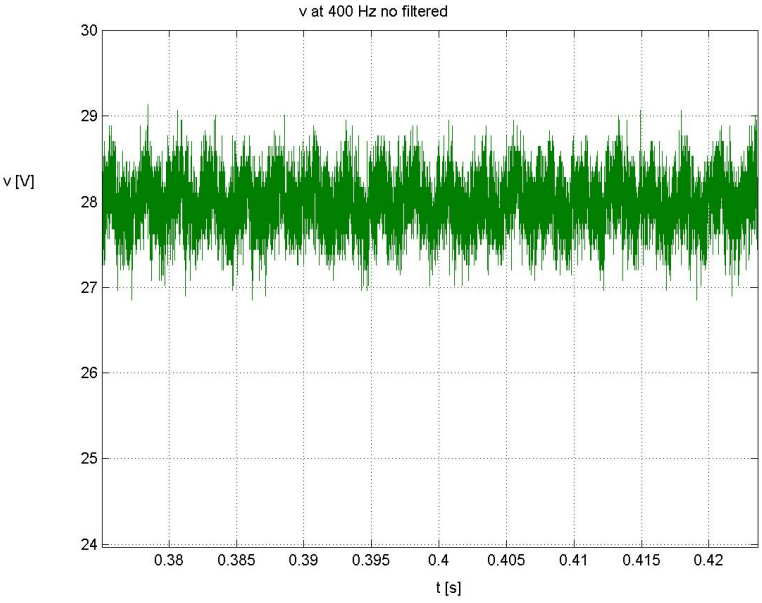

Fig 5.16 – Real time voltage at 400 Hz not filtered

To ride over this further problem, a digital software filter has been introduced in post elaboration of captured data, always in Matlab ambient. The rule at basis of this implemented filter is focused on f.d.p. of noise, that is a Gaussian function centred on the original value. According to this statement, an average value of captured data has been calculated,, in a range compatible with sampling and operative frequency, and the results has been attributed at a range suitable small regard period of alternative wave.

A great improvement has been recorded thank to this tool adopted.

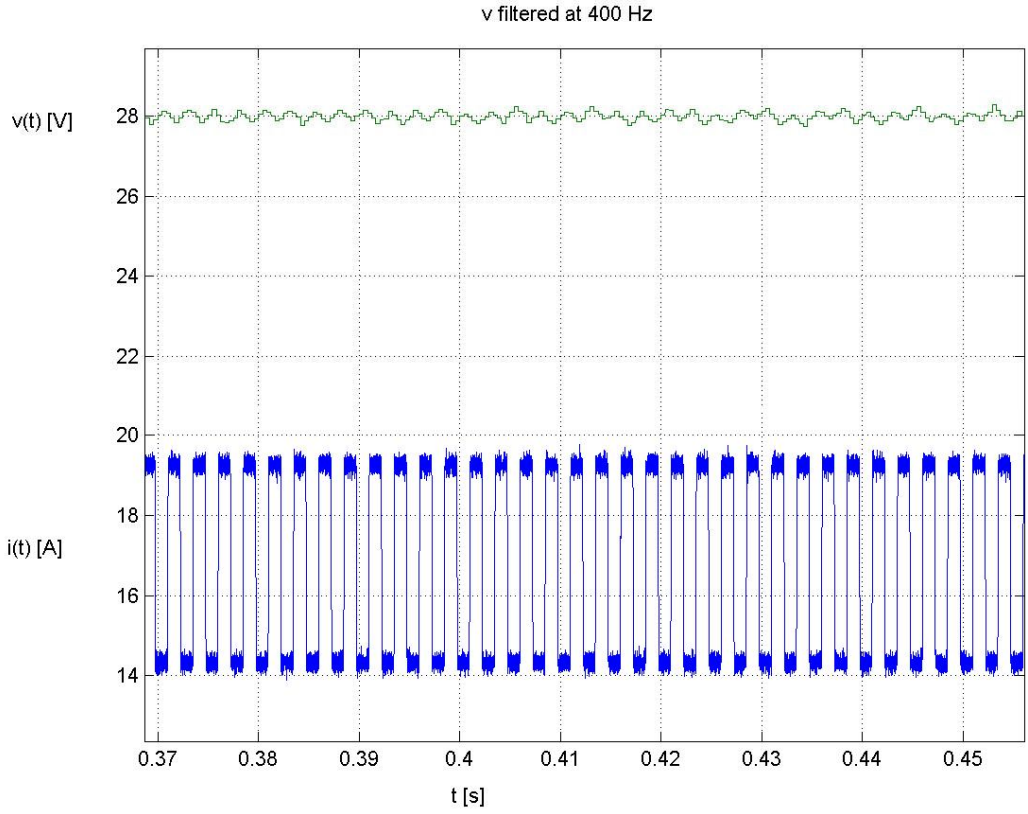

Fig 5.17 – Real time filtered voltage and current at 400 Hz

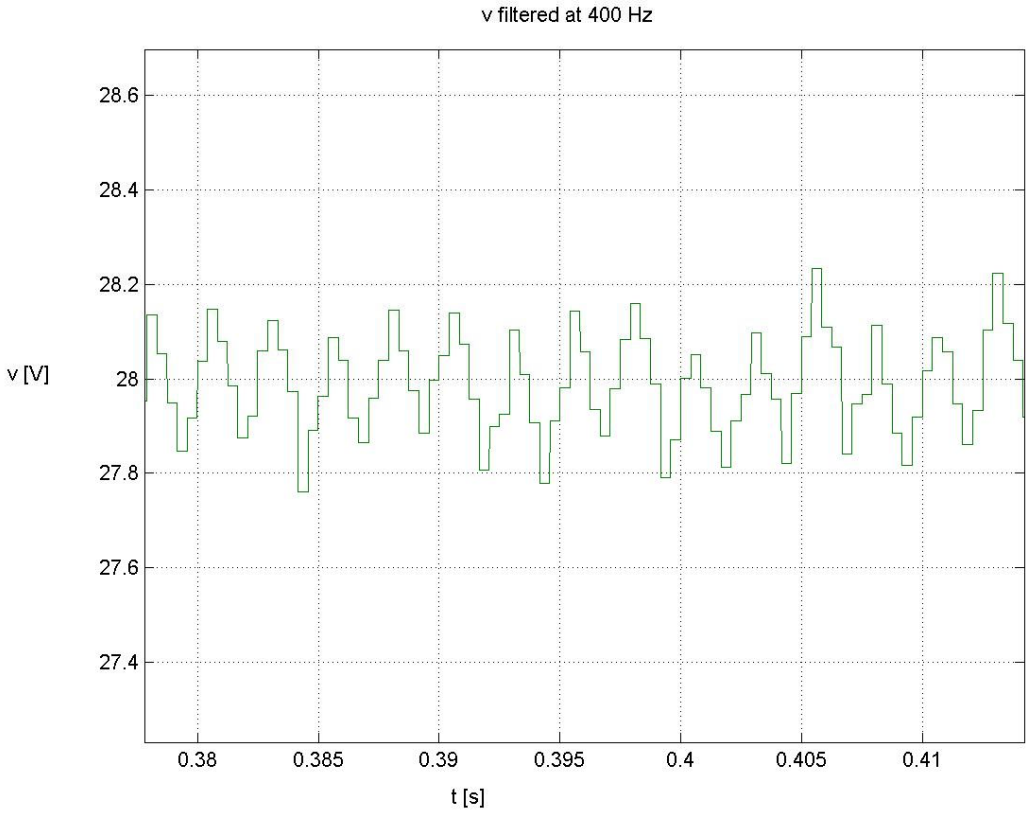

Fig 5.18 – Real time filtered voltage at 400 Hz

Main results obtained by adopting the mentioned expedient and software tool are following reported at different and main frequency state.

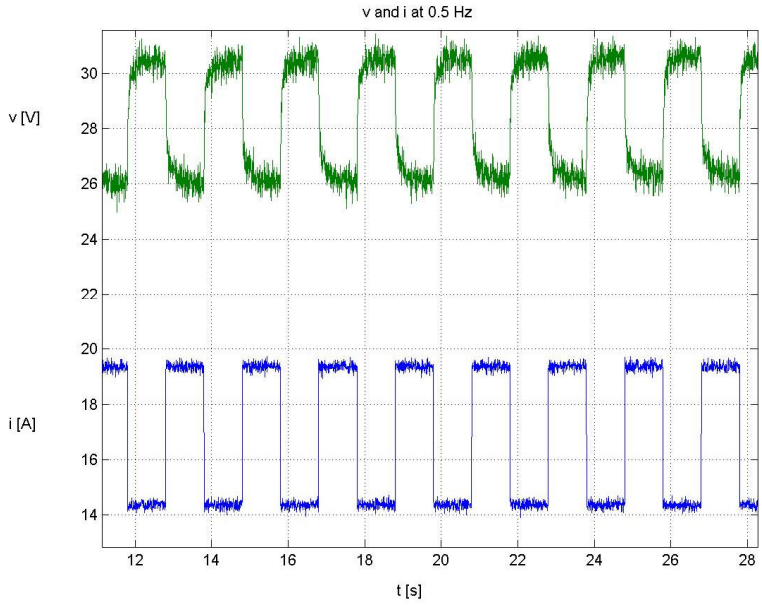

Fig 5.19 – Real time voltage and current at 0,5 Hz

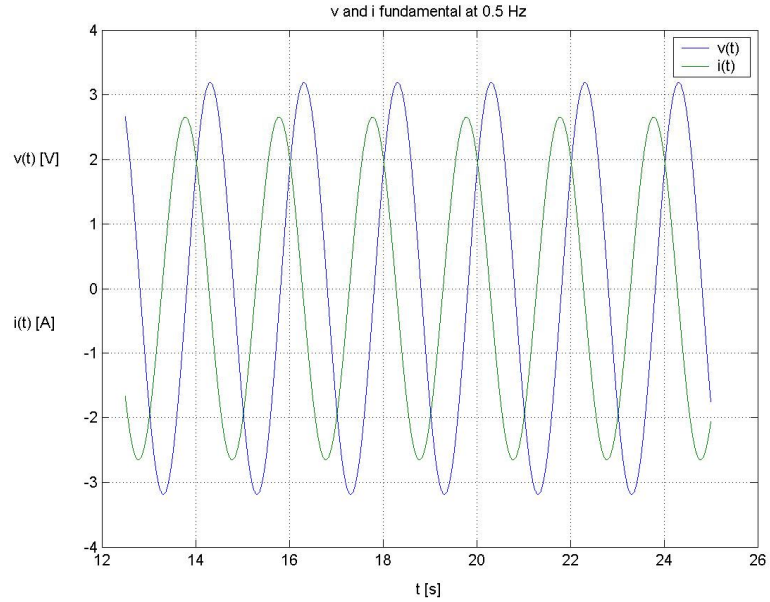

Fig 5.20 – Mean Fundamental voltage and current at 0,5 Hz

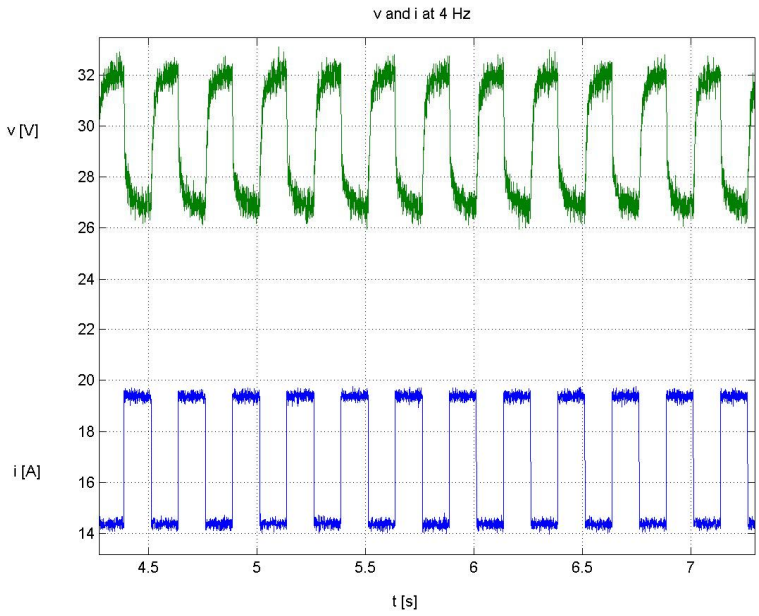

Fig 5.21 – Real time voltage and current at 4Hz

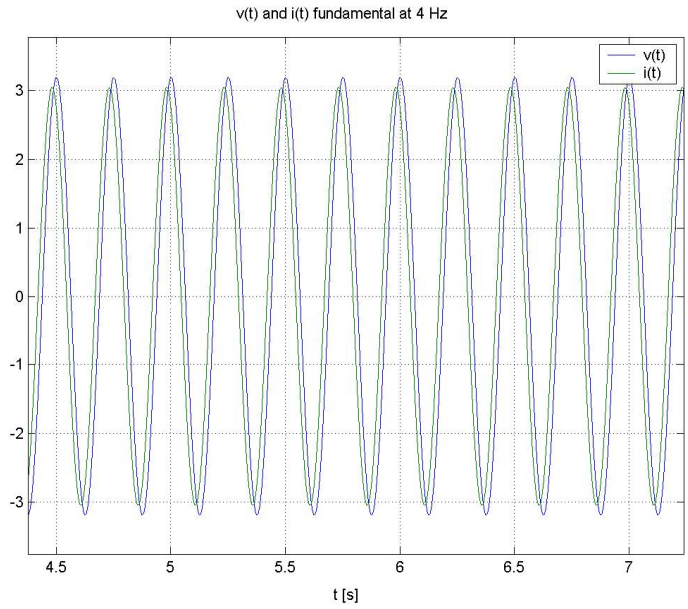

Fig 5.22 – Mean Fundamental voltage and current at 4 Hz

All the proofs performed has been focused on the target of obtaining the fuel cell equivalent impedance Nyquist graph, as simulated on the virtual model of chapter IV. Obviously, to reach this result, it has been necessary getting adapted point value in complex field, in order to fit the exact trend of graph representative the fuel cell impedance.

Here the experimental Nyquist is reported.

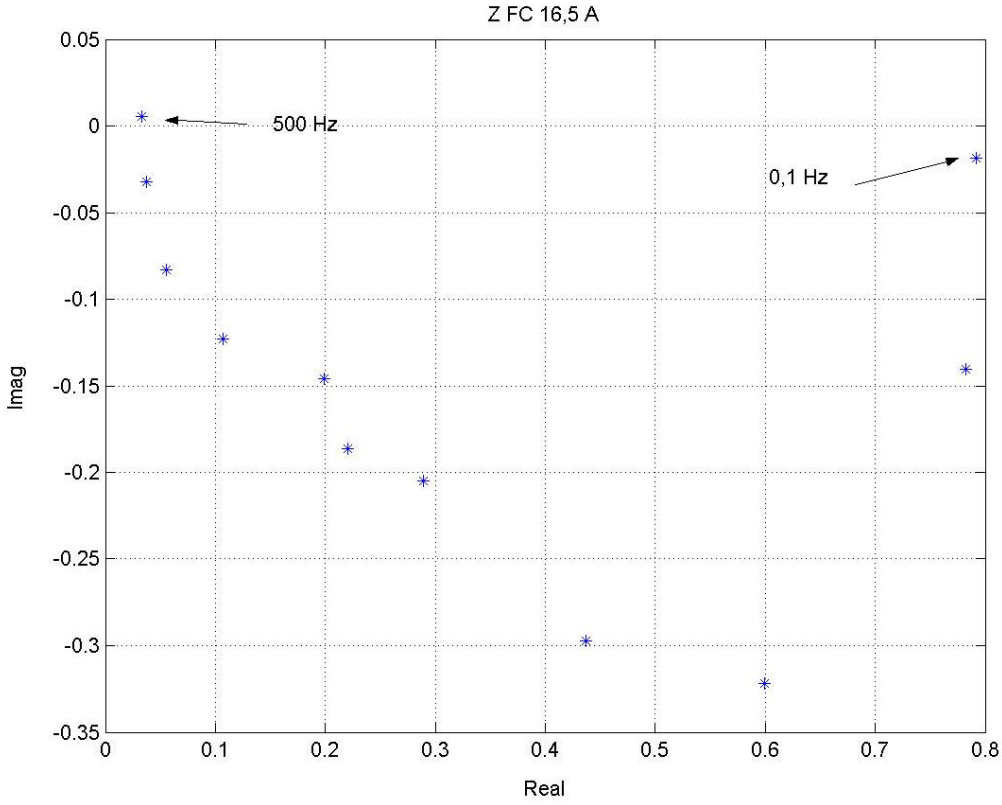

Fig 5.23 – Real post-elaborated Nyquist diagram at 16,5 A

As in static analysis, a parameter fitting has been leaded for dynamic elements. The manual iterative computation has given back an equivalent capacity value of 0,0048 F. Using this and previous static data, the following Nyquist graphic fitting has been obtained.

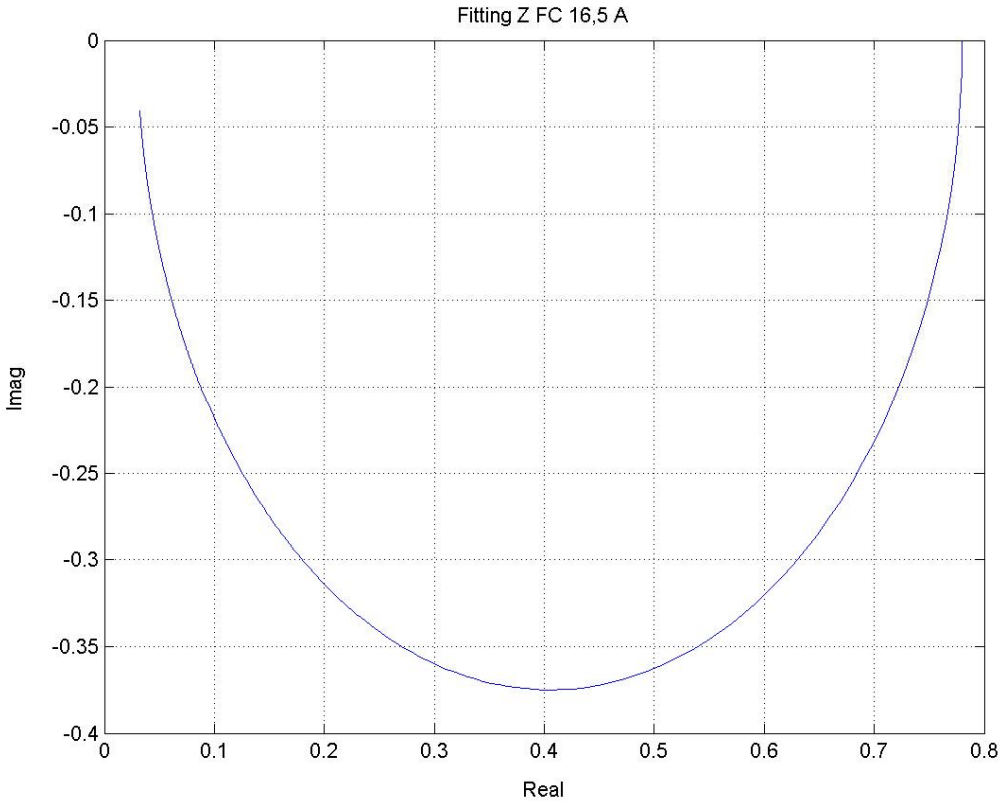

Fig 5.24 – Fitted Nyquist diagram at 16,5 A by using Randles circuit

Like in theoretical model, analyzed in chapter IV, Randles and Warburg models have been compared. The manual iterative fitted value for Warburg parameter are the following:

Rw = 0,35

Tw = 0,09

Φw = 0,7

In figure 5.25 is reported Nyquist fitted diagram.

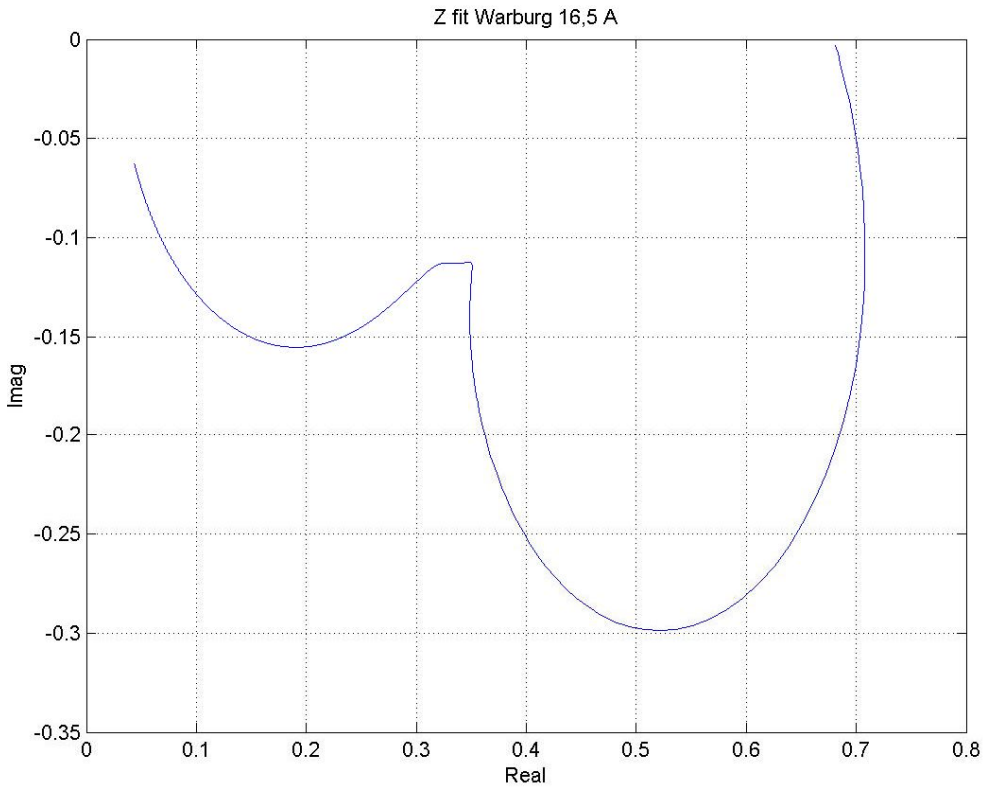

Fig. 5.25 – Nyquist diagram fitted using Warburg model

It is easy to note that also shape is different between the two Nyquist diagram, above all for the discontinuity at 50 Hz introduced by Warburg impedance.

Like in virtual case, Warburg model has given back smaller error, compared in every point with real curve, as can be observed in figure 5.26 and 5.27, where real, imaginary and module of error is reported, at every frequency.

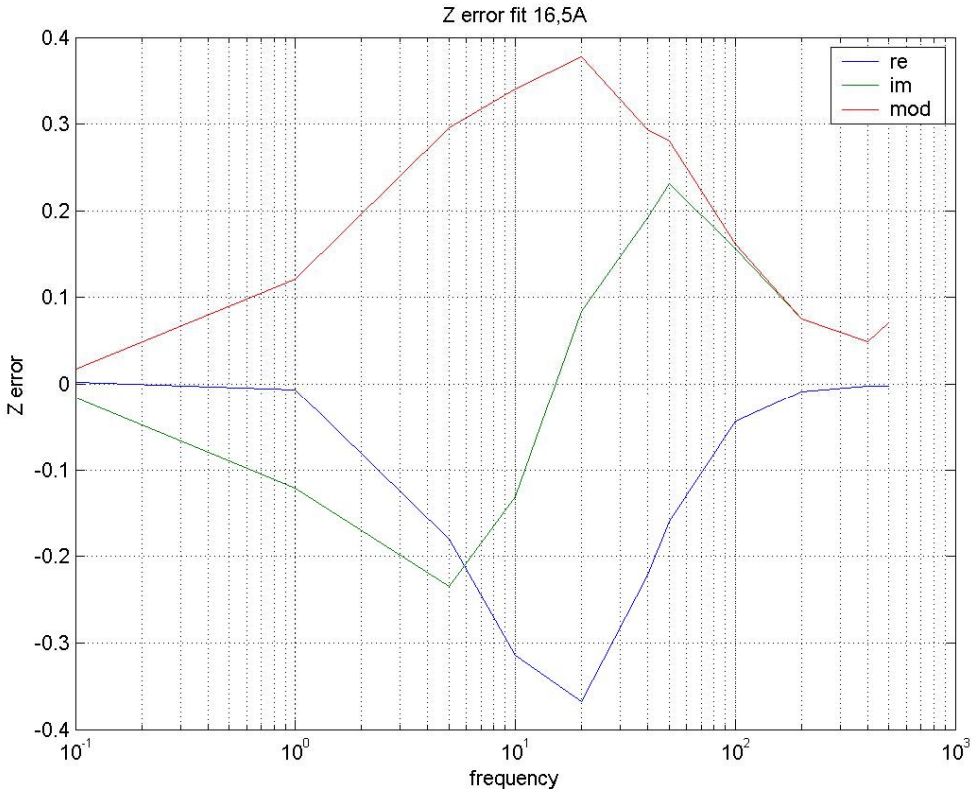

Fig. 5.26 – Error between real Nyquist diagram and Randles model fitted one

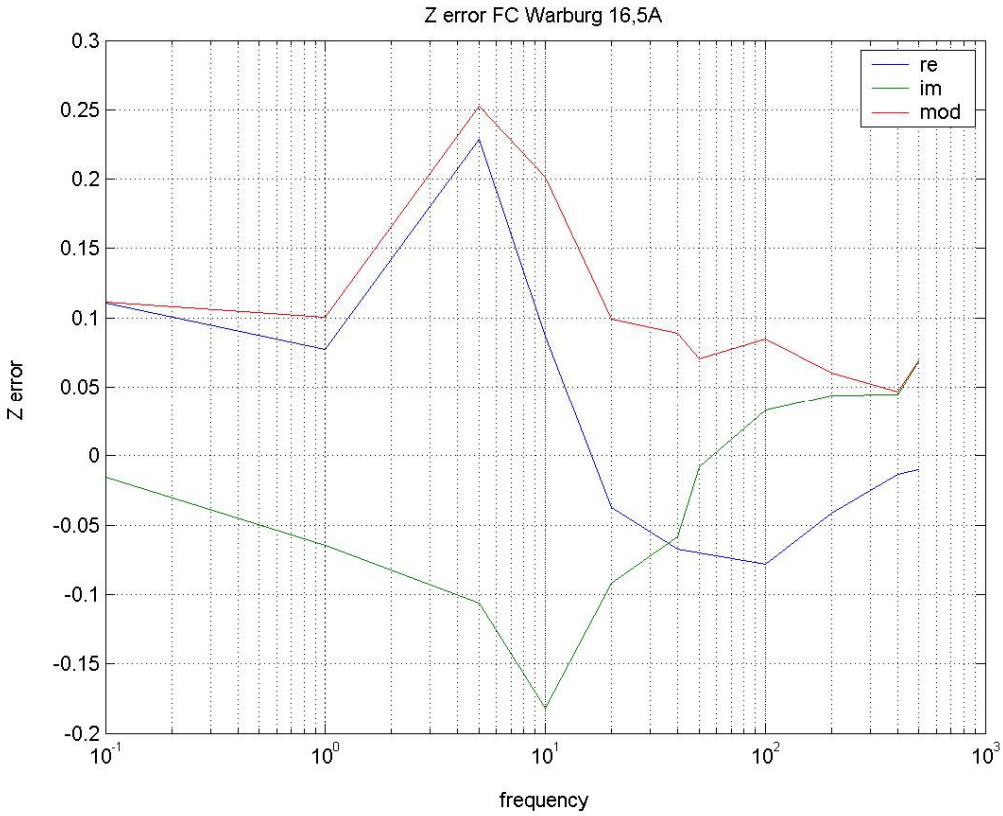

Fig. 5.27 – Error between real Nyquist diagram and Warburg model fitted one

Width of error is, in every case, due to the absence of a numerical iterative method implemented. In fact, for the early mentioned reasons, not only Randles model parameters have been obtained by manual search, but also Warburg parameters has been obtained by varying values on the basis of change of shape and scale of Nyquist diagram, that is following minor gap of real and imaginary impedance at various frequencies.

For real Nyquist curve, as for previous cases, a polynomial interpolation has been conducted, but in a first time, the set of point has been divided in two part, before and later the 50 Hz point, because a clear discontinuity is present at this value, so that the graph can be compared to two semicircle, that is two 2 degree polynomial approximation.

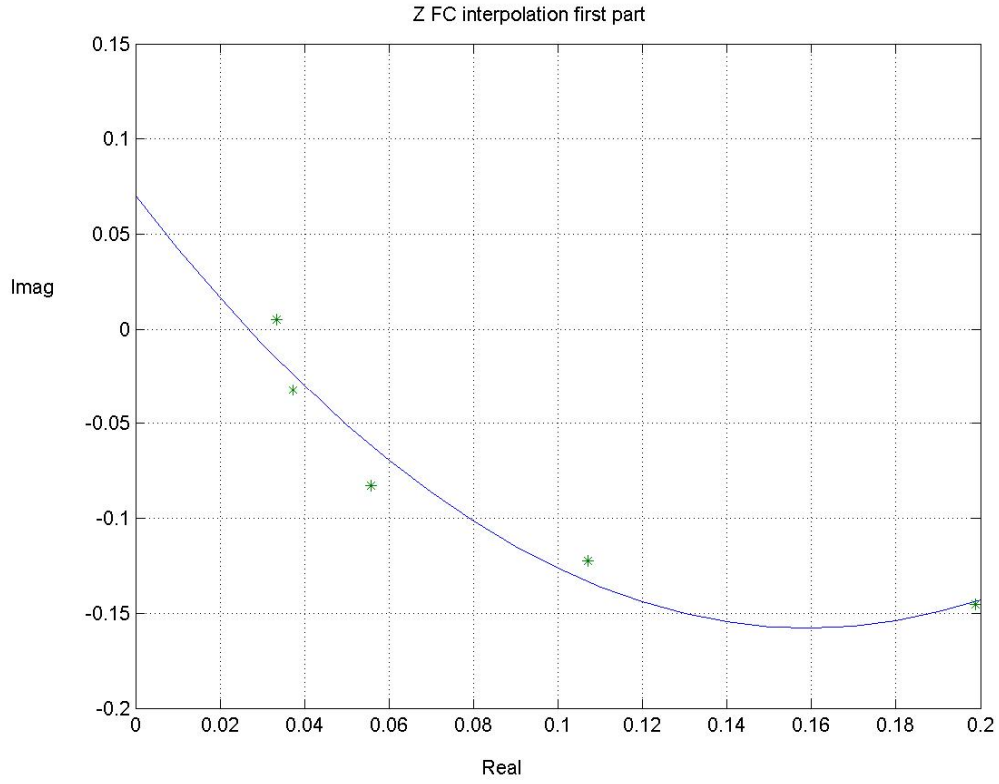

Fig 5.28 – Quadratic fitted Nyquist diagram at 16,5 A at high frequencies

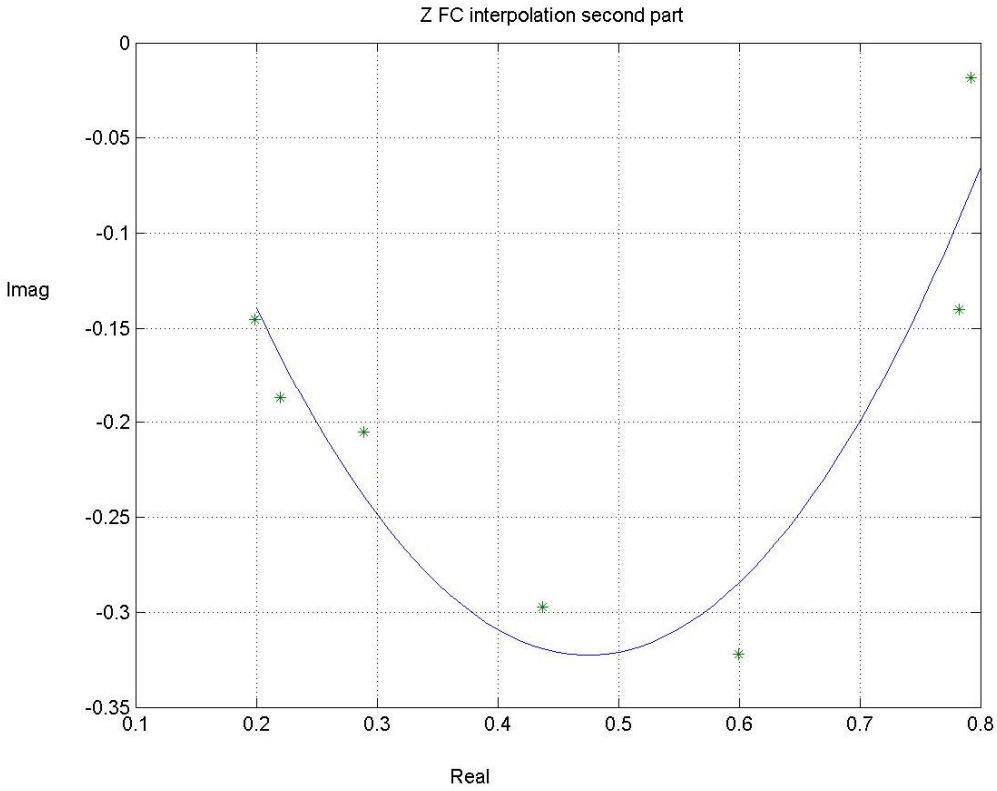

Fig 5.29 – Quadratic fitted Nyquist diagram at 16,5 A at low frequencies

Instead by applying 5 degree polynomial at all data contemporaneously the following equation has been obtained, where discontinuity point becomes an inflection point:

$$V = - 15*I^5 + 42*I^4 - 38*I^3 + 14*I^2 - 2.9*I + 0.061$$

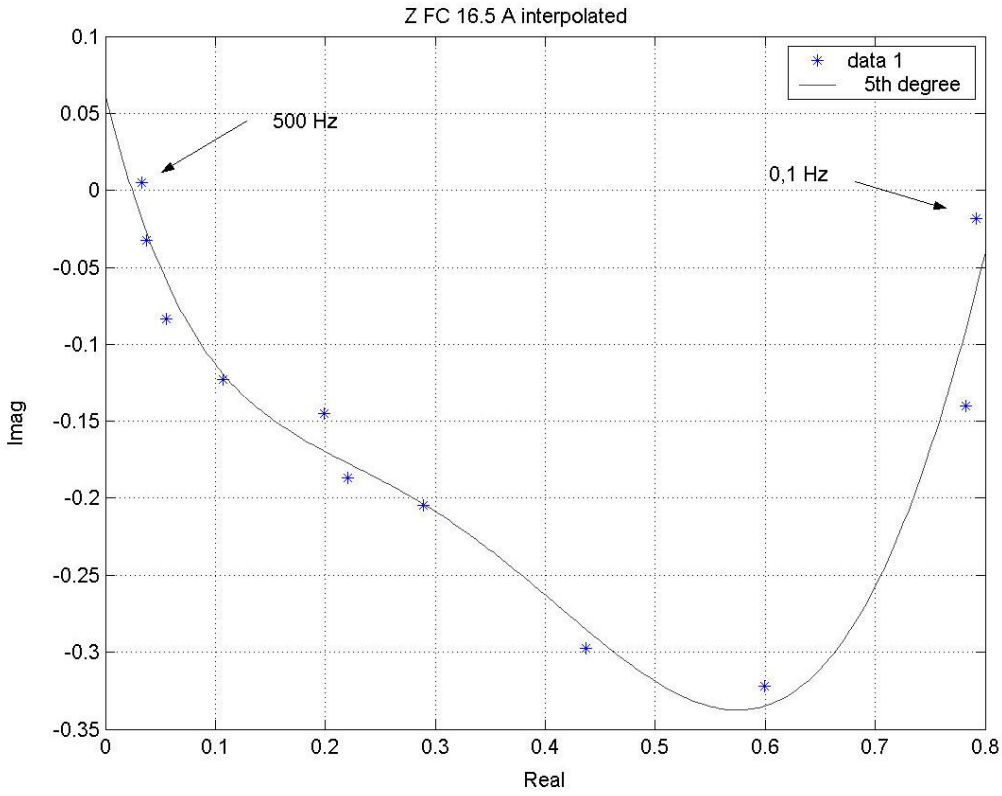

Fig 5.308 – Polynomial fitted Nyquist diagram at 16,5 A

The same proofs have been accomplished by fixing at 9,5 A the current value with a 2,5A as ripple width.

All tools used and consideration expressed for the previous case remain valid for the following one.

Here is reported the sampling exemplified at 20 Hz.

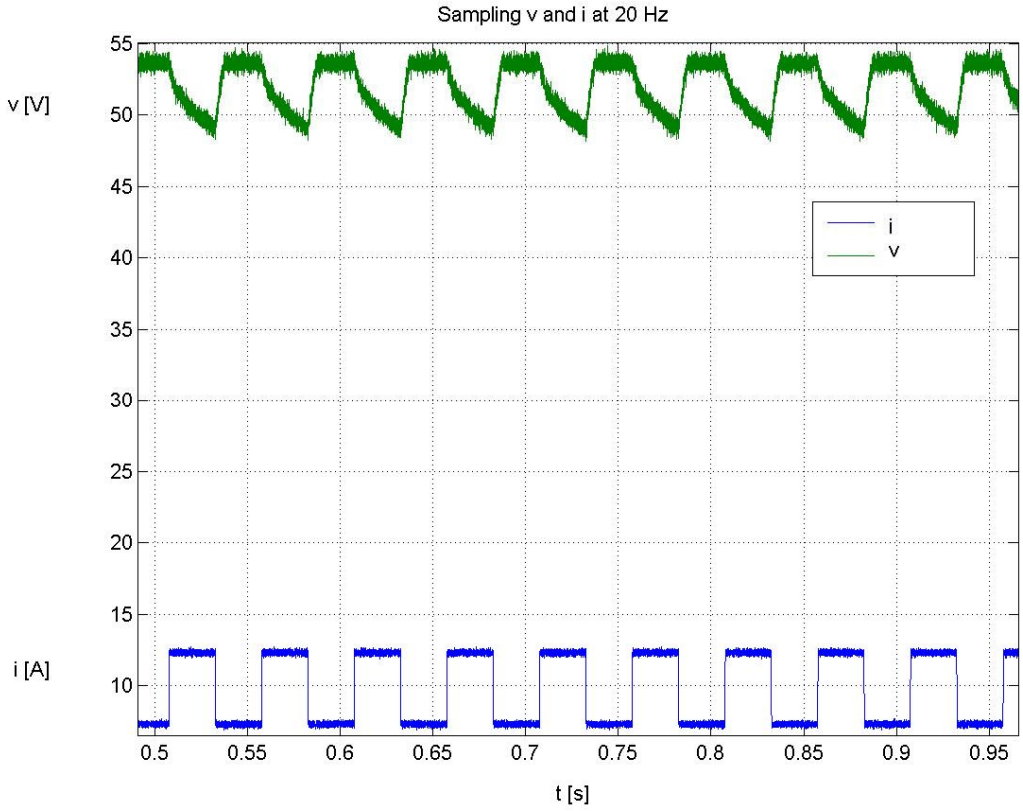

Fig 5.31 – Real time current and voltage at 20 Hz

The Fourier analysis at constant mean magnitude and angle returned the following graph for current and voltage.

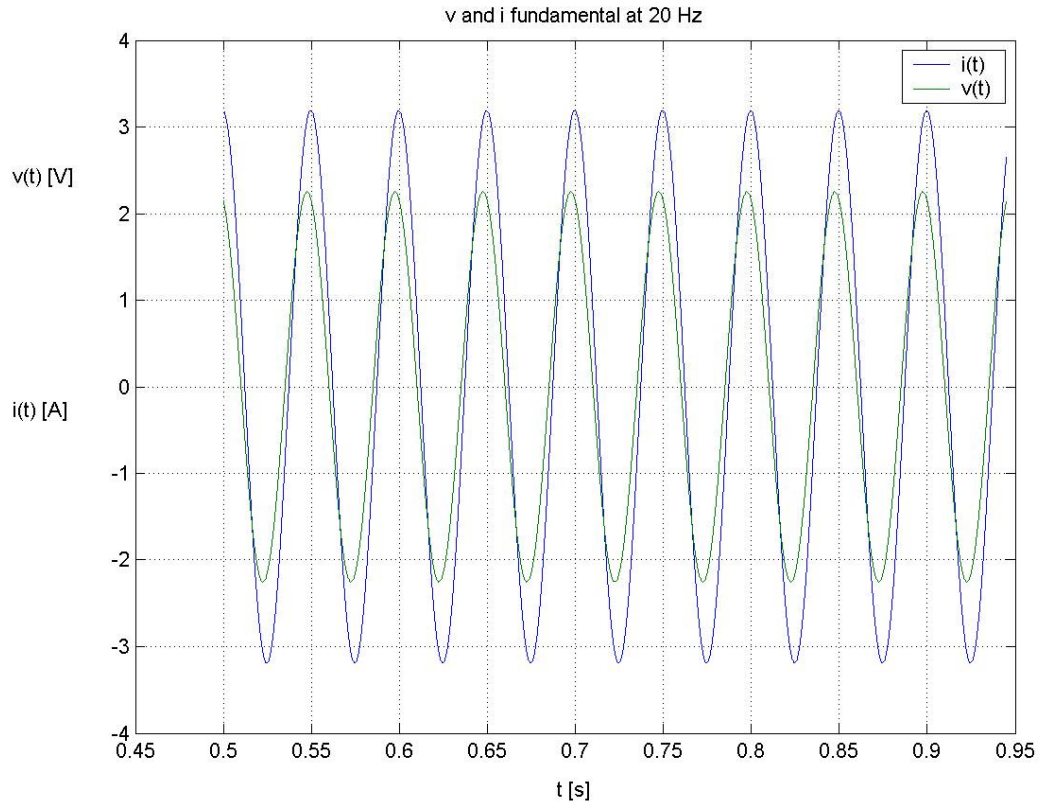

Fig 5.32 – Mean fundamental current and voltage at 20 Hz

It is easy to note that at lower current equivalent impedance value grows up, and so also voltage ripple shows larger width.

Sampling at different square wave current frequency, into an enough large range, the equivalent impedance at the considered current the relative Nyquist graph has been obtained:

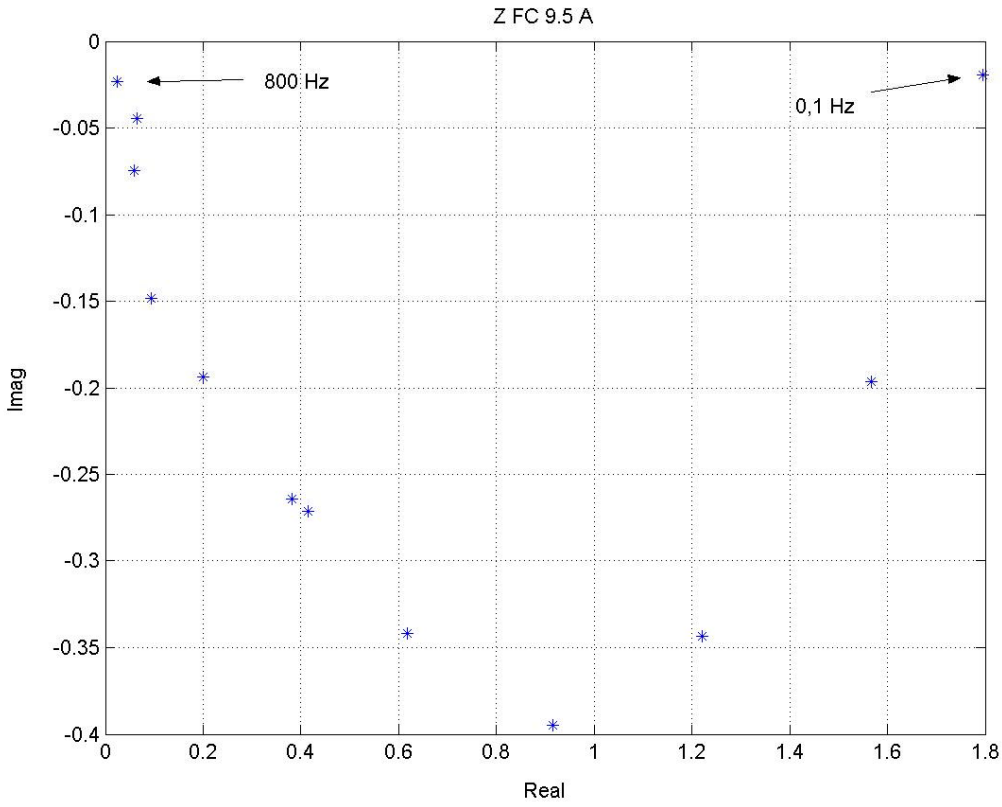

Fig 5.33 – Real post-elaborated Nyquist diagram at 9,5 A

Nyquist diagram obtained from fitting data is very similar to real one, and it is following reported.

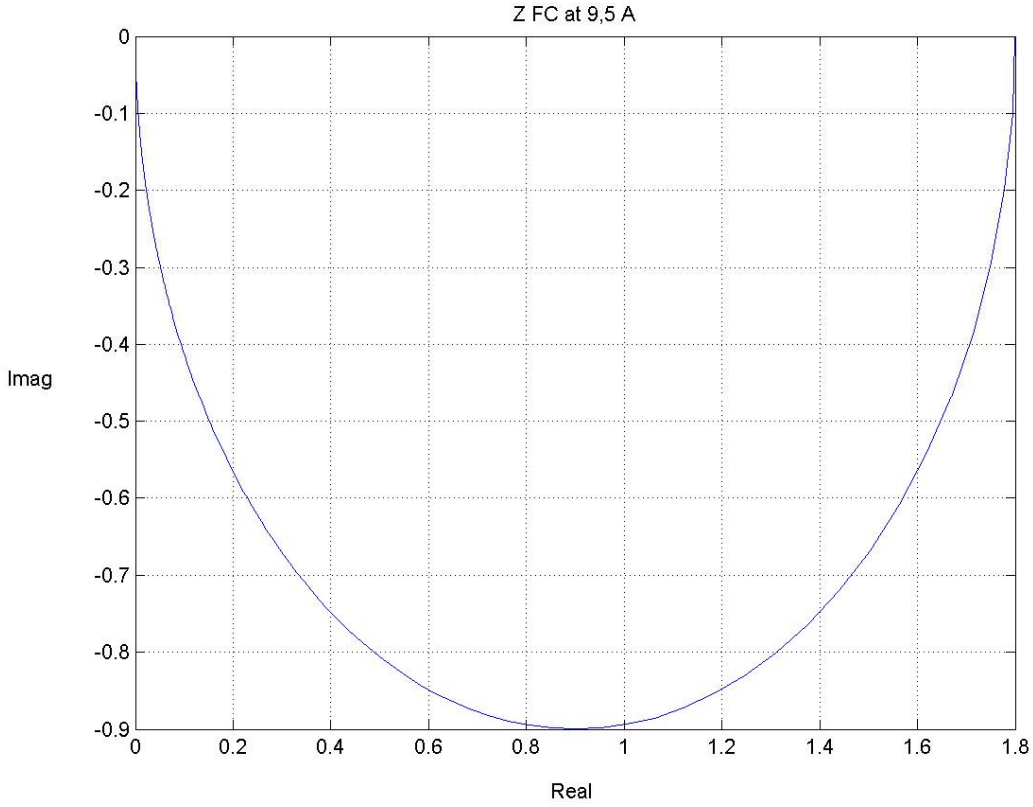

Fig 5.34 – Fitted Nyquist diagram at 9,5 A by using Randles circuit

It is a classical RC Nyquist diagram, but compared to real one, it is easy to note a great gap in middle part, due to not so linear characteristic and other influence factors. This gap is evident in every research work, where theoretical model is compared to real one [14 – 15].

The error, related to real graph, is following reported.

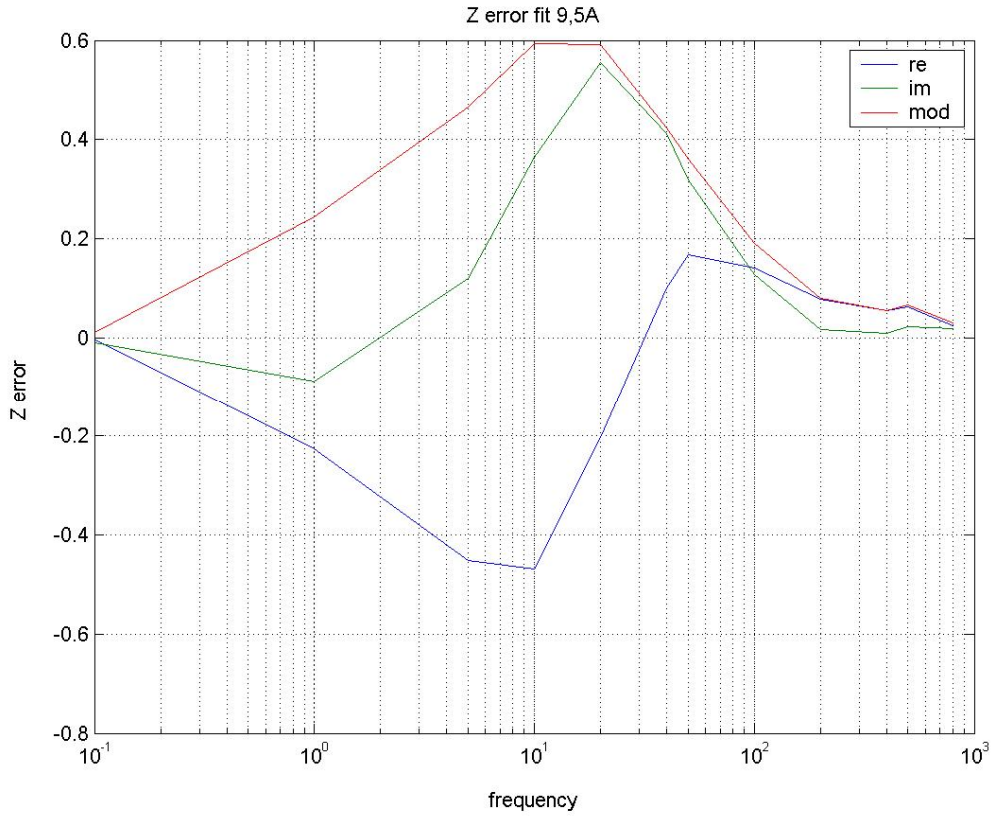

Fig. 5.35 – Error between real Nyquist diagram and Randles model fitted one

It is easy to note that around 10 Hz error is very width, but it is not very considerable because it decreases over 100 Hz, and usual field application is always located over this frequency. Moreover, usual part of characteristic useful in general application is the ohmic one, where errors are very reduced (Fig. 5.27).

Curve flattening at 9,5 A has been obtained by an analytical expedient, that, unfortunately, can't be represented by an equivalent electrical component. The consequent graph is following reported just like analytical result.

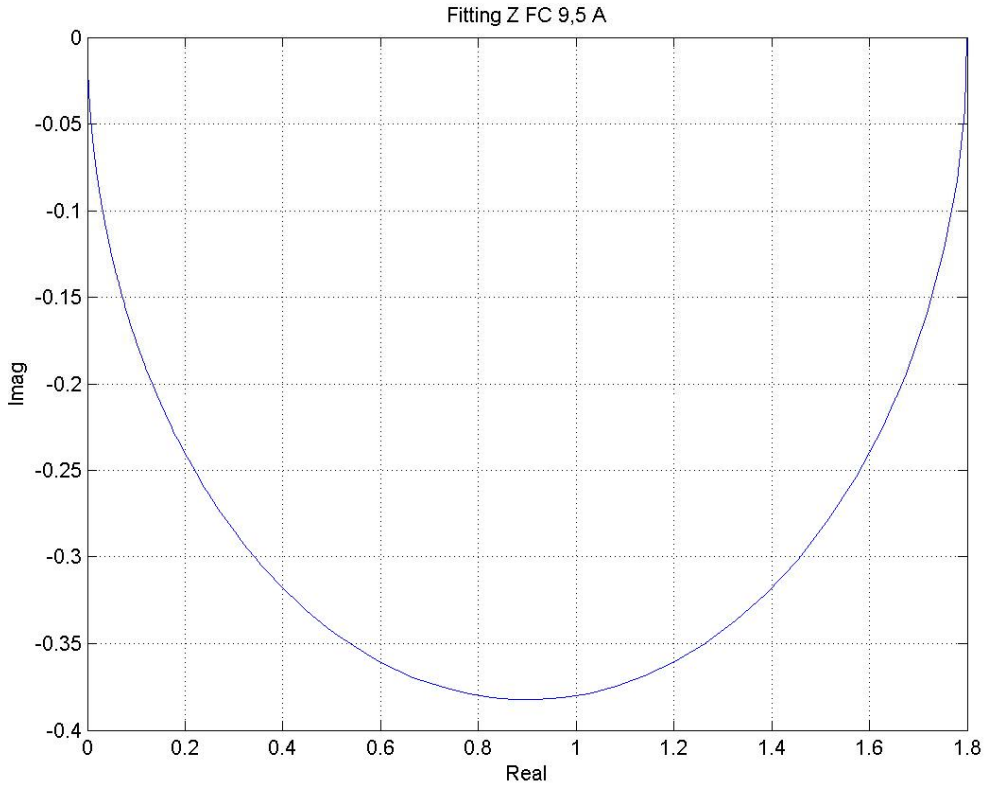

Fig 5.36 – Fitted Nyquist diagram flattened at 9,5 A by using Randles circuit

The real curve has been interpolated just by one polynomial because, differently from previous case, discontinuity points are not present, and the whole graph can be assimilate to a single semicircle (flattened for early mentioned reasons), that is a second degree equation, like expected for an RC circuit (chapter III):

$$V = 0.45*I^2 - 0.81*I - 0.026$$

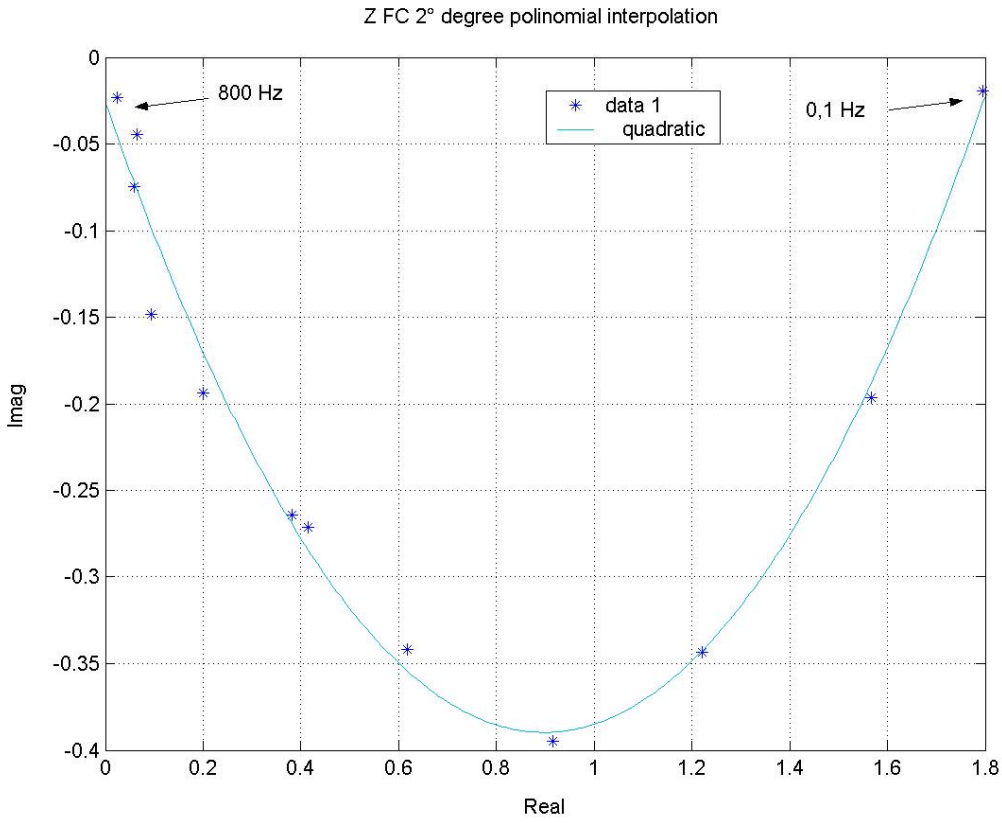

Fig 5.37 – Quadratic fitted Nyquist diagram at 9,5 A

As expected impedance value has grown up respect to 16.5 A case for the reason expressed in chapter III and following discussed in comparison between theoretical and real graphs.

CHAPTER V - ELECTROCHEMICAL IMPEDANCE SPECTROSCOPY EXPERIMENTAL RESULTS

Synthesis considerations

The data adopted in the virtual model have been choice on the model of table reported in the publication “Sensitivity Analysis of the Modelling Parameters Used in Simulation of Proton exchange Membrane Fuel Cells”, whose model is very similar to that implemented in Matlab simulation of chapter IV, less than the remarkable difference of using a new parameter, which takes into account the diffusion phenomena shown at high current value.

In the mentioned work, the equivalent electrical model and dynamic response to step current input are treated very well, but few considerations are reported about contemporaneous presence of continuous and alternative current on the load, and, consequently, about the real and correct interpretation of complex impedance model. Otherwise, the reported captured data do not express Fuel Cell behaviour into all the interesting range.

This kind of experiment has faced in the publication “PEMFC Diagnostics and Modelling by Electrochemical Impedance Spectroscopy”, where a similar laboratory instrumentation has been assembled, and the same operative mode of execution has been leaded, but the right interpretation of alternative results misses. However, the frequency domain proofs are complete, and they validate the qualitative results reported in this chapter, and the proportionally of impedance, voltage and current, taking into account the different size of Fuel Cell used. Also diffusion effect is clearly visible, but a theoretical analytical model misses, just a qualitative interpretation of physical

phenomena is leaded, instead in chapter III and IV of this work, diffusion is represented by an analytical trigonometric equation, that introduces a new electrical component in a complete equivalent circuit. Otherwise the presence of diffusion, just at high current level, has an analytical interpretation in the small size of Warburg impedance, that becomes influent just when other electric parameter of equivalent impedance decrease their magnitude, at high current.

All that is validated not only by real capturing executed in this work, but also in other research work as [14] and [15].

CHAPTER VI - CONCLUSIONS

CHAPTER VI – CONCLUSIONS

This work focuses on the theoretical analysis and experimental validation of a Fuel Cell Electrical source. The aim of the work is to examine the equivalent electrical circuits proposed in literature, in order to take into account the operating conditions of the source with or without a dedicated converter.

The work starts from the analysis of the physical aspects of the source, focusing on the main phenomena which characterise the source behaviour. The effects of activation, concentration and ohmic phenomena are examined, to define the source analytical model able to take into account DC and AC operating conditions.

In the final part of the work, experimental tests are performed. A laboratory stations have been equipped with a 1 kW FC source and an electronic load, able to set variable operating conditions of the electrical source. Analyses are performed using the Electrochemical Impedance Spectroscopy (EIS) method. The application of EIS, through the laboratory instruments, gives back an interesting way of getting information about the fuel cell stack. In fact, for its simplicity, it could be implemented also in real time for diagnostic application, by using ordinary microprocessor, able to execute not so complex iterative search of parameter.

The importance of getting an equivalent circuit model, is already note to everyone, because of numerous applications that Fuel Cells can have, for which e theoretical model is necessary. Moreover, if we consider the possibility of obtaining in simple way the “actual set” of equivalent parameter, the potential of this work results evident. Above all, in couple with converters, this model and method is useful to preliminary

sizing. Also for hybrid application, it is useful to choice the characteristic of sources and dynamic response.

All that can be considered well-founded not only thank to virtual and real laboratory experimentation, but also thank to proofs executed in every research work, that make this results and conclusions of general application.

BIBLIOGRAPHY

BIBLIOGRAPHY

[1] Laurencelle F., Chahine R., Hamelin J., Agbossou K., Fournier M., Bose T. K. and Laperriére A., 2001, "Characterization of a Ballard MK5-E Proton Exchange Membrane Fuel Cell Stack", Fuel Cells, 1 (1), pp. 66-71.

[2] Knights S.D., Colbow K. M., St-Pierre J., Wilkinson D. P., 2004, "Aging mechanisms and lifetime of PEFC and DMFC", Journal of Power Sources 127, pp. 127–134.

[3] Fowler M.W, Mann R.F., Amphlett J.C., Peppley B.A., Roberge R.P.R., 2002, "Incorporation of voltage degradation into generalized steady-state electrochemical model for a PEM fuel cell", Journal of Power Sources 106, pp.274–283.

[4] Hector R. Colòn-Mercado, Hansung Kim, Branko N. Popov: "Durability study of Pt3Ni1 catalysts as cathode in PEM fuel cells", Electrochemistry Communications 6 (2004) 795–799.

[5] Dennis E. Curtin, Robert D. Lousenberg, Timothy J. Henry, Paul C. Tangeman, Monica E. Tisack: "Advanced materials for improved PEMFC performance and life", Journal of Power Sources 131 (2004) 41–48.

[6] Berndt D., 2003, Maintenance-Free Batteries Based on Aqueous Electrolyte, Third Edition, Research Studies Press LTD, Baldock, England

[7] Buonarota A., Grattieri W., Camozza A., Report CESI *SFR-A1/018349*, www.cesi.it

[8] Jiang Z., Gao L., Blackwelder M. J., Dougal R. A., 2004, "Design and experimental tests of control strategies for active hybrid fuel cell/battery power sources", Journal of Power Sources 130, pp. 163–171.

BIBLIOGRAPHY

[9] Schupbach R.M., Balda J.C., 2003, "The role of ultracapacitors in an Energy Storage unit for vehicle power management", Vehicular Technology Conference, Vol. 5, pp. 3236-3240.

[10] L. Gao, Z. Jiang, R. Dougal: "Evaluation of Active hybrid fuel cell/batetry power sources", IEEE Trans. On Aerospace and Electronic Systems, Vol.41, No. 1, January 2005

[11] Schupbach R.M., Balda J.C., Zolot M., Kramer B., 2003, "Design methodology of a combined battery-ultracapacitor energy storage unit for vehicle power management", Power Electronics Specialist Conference, Vol. 1, pp. 88-93

[12] Sensitivity Analysis of the Modelling Parameters Used in Simulation of Proton Exchange Membrane Fuel Cells J. M. Corrêa *(Student Member*, *IEEE)*, F. A. Farret, V. A. Popov, M. Godoy Simões *(Senior Member*, *IEEE)*

[13] "Algorithm Development for Electrochemical Impedance Spectroscopy Diagnostics in PEM Fuel Cells" By Ruth Anne Latham; BSME, Lake Superior State University, 2001; department of Mechanical Engineering.

[14] PEMFC Diagnostics and Modelling by Electrochemical Impedance Spectroscopy C. Brunetto*, G. Tina", G. Squadrito** and **A.** Moschetto** * Universita degli Studi di Catani Dipartimento di Ingegneria Elettrica Elettronica e dei Sistemi, Catania, Italy **CNR/ITAE, Messina, Italy (cbrune@diees.unict.it, gtina@diees.unict.it, squadrito@itae.cnr.it, moschetto@itae.cnr.it).

[15] "Simultaneous electrochemical impedance spectroscopy of single cells in a PEM fuel cell stack" Alex Hakenjos , Marco Zobel, Jan Clausnitzer, Christopher Hebling;

BIBLIOGRAPHY

Fraunhofer Institute for Solar Energy Systems (ISE), Heidenhofstr. 2, 79110 Freiburg, Germany; Available online 4 January 2006.

[16] "Electrochemical impedance spectra of solid-oxide fuel cells and polymer membrane fuel cells" N. Wagner, W. Schnurnberger, B. Muller and M. Lang; Insitute fur technische Thermodynamik, Pfaffenwaldring 38-48, D-70569 Stuttgart, Germany.

[17] "Minimization of on-board Fuel Cell Power Sources introducing aging constrains" M. Pagano, *Member, IEEE*, G. Velotto, and A. Zingariello.

Special thanks to:
Ing. Mario Pagano, who enabled fulfilment of this work.
My family, for their continuous support.